

Glutarate regulates T cell metabolism and anti-tumour immunity

Received: 31 October 2022

Accepted: 3 July 2023

Published online: 21 August 2023

 Check for updates

Eleanor Minogue¹, Pedro P. Cunha¹, Brennan J. Wadsworth²,
Guinevere L. Grice³, Shiv K. Sah-Teli⁴, Rob Hughes¹, David Bargiela¹,
Alessandro Quaranta⁵, Javier Zurita⁵, Robin Antrobus⁶, Pedro Velica²,
Laura Barbieri^{1,2}, Craig E. Wheelock^{5,7}, Peppi Koivunen⁴,
James A. Nathan³, Iosifina P. Foskolou¹ & Randall S. Johnson^{1,2}✉

T cell function and fate can be influenced by several metabolites: in some cases, acting through enzymatic inhibition of α -ketoglutarate-dependent dioxygenases, in others, through post-translational modification of lysines in important targets. We show here that glutarate, a product of amino acid catabolism, has the capacity to do both, and has potent effects on T cell function and differentiation. We found that glutarate exerts those effects both through α -ketoglutarate-dependent dioxygenase inhibition, and through direct regulation of T cell metabolism via glutarylation of the pyruvate dehydrogenase E2 subunit. Administration of diethyl glutarate, a cell-permeable form of glutarate, alters CD8⁺ T cell differentiation and increases cytotoxicity against target cells. In vivo administration of the compound is correlated with increased levels of both peripheral and intratumoural cytotoxic CD8⁺ T cells. These results demonstrate that glutarate is an important regulator of T cell metabolism and differentiation with a potential role in the improvement of T cell immunotherapy.

T cell activation initiates the process whereby quiescent, naive T cells differentiate into rapidly proliferating effector cells. This transition involves a profound and dynamic metabolic reprogramming. After the resolution of an immune response, some T cells transition to memory cells: these cells are primed for rapid recall responses. Most of the remaining T cells become exhausted and then die through apoptosis^{1,2}. T cell differentiation, memory cell formation and T cell survival are regulated by many intrinsic factors, including transcriptional and epigenetic regulation^{1,3–5}. These processes are also regulated by extrinsic factors, including both nutrient and oxygen availability^{6–10}.

In recent years, our laboratory and others illustrated the importance of the S enantiomer of 2-hydroxyglutarate (S-2HG) in determining T cell fate^{11–13}. We showed that supplementation of T cell cultures

with esterified forms of S-2HG enhances T cell immunotherapy in preclinical models, where it acts by promoting the development of central memory T (T_{CM}) cells. 2HG and the metabolites succinate and fumarate are structural analogues of α -ketoglutarate (α KG) and all can act as competitive inhibitors of α KG-dependent dioxygenases (α KGDDs)^{14–18}. These enzymes have essential roles in many cellular processes, and there are currently over 60 identified^{19–21}. S-2HG itself has been shown to exert many of its modulation of T cell function via competitive inhibition of specific α KGDDs¹¹.

In this study, we sought to determine whether molecules structurally similar to S-2HG might exert similar effects on T cell differentiation and function. We describe our finding that glutarate is found at significant levels in activated T cells and is a potent inhibitor of several

¹Department of Physiology, Development and Neuroscience, University of Cambridge, Cambridge, UK. ²Department of Cell and Molecular Biology, Karolinska Institutet, Stockholm, Sweden. ³Cambridge Institute of Therapeutic Immunology & Infectious Disease, Department of Medicine, Jeffrey Cheah Biomedical Centre, Cambridge Biomedical Campus, University of Cambridge, Cambridge, UK. ⁴Biocenter Oulu, Faculty of Biochemistry and Molecular Medicine, Oulu Centre for Cell-Matrix Research, University of Oulu, Oulu, Finland. ⁵Unit of Integrative Metabolomics, Institute of Environmental Medicine, Karolinska Institutet, Stockholm, Sweden. ⁶Cambridge Institute for Medical Research, University of Cambridge, Cambridge, UK. ⁷Department of Respiratory Medicine and Allergy, Karolinska University Hospital, Stockholm, Sweden. ✉e-mail: randall.johnson@ki.se

αKGDDs. In addition, we found that glutarate can strongly influence cellular metabolism and T cell differentiation.

Glutarate, in its coenzyme A (CoA) form, is an important intermediate of both tryptophan and lysine catabolism^{22,23}. Glutarate and glutaryl-CoA arise during the final stages of the kynurenine pathway, a catabolic process which has many demonstrated roles in immunoregulation; however, curiously, glutarate has not been extensively studied in an immune context previously. Glutaryl-CoA can be broken down to either crotonyl-CoA by the enzyme glutaryl-CoA dehydrogenase (GCDH), or form glutarate²⁴. The glutarate to glutaryl-CoA reaction is mediated by succinyl-CoA:glutarate-CoA transferase (SUGCT)²⁵.

The ratio of crotonyl-CoA to glutarate is highly regulated, and excessive glutarate accumulation can be cytotoxic²⁶. Previous work on the cellular and physiological roles of glutarate has almost exclusively focused on patients with loss of function mutations in the GCDH enzyme, which results in excessive glutarate accumulation. These patients present with the metabolic disorder glutaric aciduria type 1 (GA1). This autosomal recessive genetic disorder has varying outcomes, and these range from mild to severe developmental disorders and to seizure syndromes^{26–29}.

Other than work on GA1, there is a very limited literature describing the physiological or metabolic role of glutarate. We show in this study that glutarate is present at significant levels in activated CD8⁺ T cells, and that these levels fluctuate greatly during activation. We additionally illustrate that glutarate controls the activity of the pyruvate dehydrogenase complex (PDHc) via post-translational modification glutarylation. We show that glutarylation disrupts lipoylation of the PDHc E2 subunit and reduces PDHc catalytic activity. Together, our findings highlight glutarate as an important metabolite with significant T cell modulatory capacity.

Results

Glutarate is an endogenous regulator of CD8⁺ T cell function

We first sought to investigate if compounds structurally related to 2HG could increase the T_{CM} population of CD8⁺ T cells. To carry out this analysis, we identified 19 structural analogues of 2HG; eight were commercially available and 11 were synthesized de novo for the purposes of this study (Table 1). We used esterified versions of most of the compounds used, so as to increase both potency and intracellular translocation. The octyl ester form of S-2HG was used as a positive control in these assays. We screened the compounds for effects on T cell differentiation at 400-μM levels (using the efficacy of S-2HG in CD8⁺ T cells as a guide¹¹) in culture media during the process of activation of isolated primary murine CD8⁺ T cells.

After 7 days of culture, we assessed the abundance of CD62L^{hi} CD44^{hi} (T_{CM}-like) T cells by flow cytometry (Fig. 1a). We additionally determined the effect of each compound on cell growth and viability (Fig. 1b and Extended Data Fig. 1a). Of the 19 test compounds assayed, only diethyl glutarate (DEG) significantly increased the abundance of CD62L^{hi}CD44^{hi} CD8⁺ T cells in our assays (Fig. 1a). Further, treatment with DEG had no negative effects on either cell viability or proliferation (Fig. 1b and Extended Data Fig. 1a). DEG increased the CD62L^{hi} CD44^{hi} T_{CM} population in a dose-dependent manner, at concentrations similar to those used with treatment with octyl ester S-2HG (Extended Data Fig. 1b).

As noted, DEG did not display any negative effects on cell growth, even at 1-mM concentrations. This contrasts with octyl ester S-2HG, which decreases cell growth from 400 μM (Extended Data Fig. 1c). Further analysis of memory populations in both mouse and human CD8⁺ T cells treated with DEG revealed that after 7 days of culture, DEG increased the T_{CM} population in both mouse and human differentiating T cells (as represented by CD62L^{hi}CD44^{hi} in mouse and CCR7^{hi}CD45RO^{hi} in human cells), and decreased effector memory T (T_{EM}) cell populations (as represented by CD62L^{lo}CD44^{hi} in mouse and CCR7^{lo}CD45RO^{hi} in human CD8⁺ T cells) (Fig. 1c,d).

Table 1 | List of test compounds (plus S-2HG) used in the screen described in Fig. 1a

Commercially available			Newly synthesized	
ID	Molecular formula	Description	ID	Molecular formula
S2HG	C ₁₃ H ₂₅ NaO ₅	(2S)-2-hydroxyglutaric acid octyl ester sodium salt	163	C ₁₂ H ₂₁ NO ₆
DSB	C ₈ H ₁₄ O ₄ S	1,4-diethyl 2-sulfanylbutanedioate	158	C ₉ H ₁₇ NO ₄
DTA	C ₈ H ₁₄ O ₄ S	Diethyl 2,2'-thiodiacetate	166	C ₁₂ H ₂₀ O ₆ S
DIM	C ₈ H ₁₅ NO ₄	Diethyl iminodiacetate	159	C ₉ H ₁₆ O ₅
DMA	C ₈ H ₁₄ O ₅	D-(+)-malic acid diethyl ester	164	C ₁₂ H ₁₉ NO ₇
DASH	C ₈ H ₁₅ NO ₄	(S)-diethyl 2-aminosuccinate hydrochloride	161	C ₈ H ₁₄ O ₅
DGA	C ₉ H ₁₇ NO ₄	L-glutamic acid diethyl ester hydrochloride	168	C ₁₃ H ₂₂ O ₆
EOA	C ₈ H ₁₃ NO ₅	N-(2-ethoxy-2-oxoacetyl)glycine ethyl ester	162	C ₁₀ H ₁₈ O ₄
DEG	C ₉ H ₁₆ O ₄	Diethyl glutarate	167	C ₉ H ₁₆ O ₄ S
			165	C ₁₂ H ₂₀ O ₇

DEG is a di-esterified form of the metabolite glutaric acid (glutarate). In the initial screen of metabolites (Figs. 1a), five compounds with diethyl-ester groups were used to increase cellular translocation, with only one, DEG, having an effect on CD8⁺ T cell differentiation. This indicates that these effects on differentiation are not likely due to treatment with diethyl group-containing compounds or the esterified ethyl groups. Additionally, we found that treatment with glutarate alone was also capable of increasing T_{CM} populations during the activation and differentiation of CD8⁺ T cells, although this was seen at higher doses after 10 days of culture (Extended Data Fig. 1d,e). This last result indicates that although exogenous glutarate may be taken up by T cells, the esterified version of glutarate is more effective at modulating CD8⁺ T cell differentiation.

To affirm that exogenous administration of DEG leads to increased intracellular glutarate levels, we performed isotope tracing of human CD8⁺ T cells treated with ¹³C₅-labelled DEG. Tracing showed that DEG is very rapidly converted into intracellular glutarate after uptake (Extended Data Fig. 1f,g). These data indicate that processing of DEG into glutarate occurs within minutes after DEG uptake. Consistent with this finding, intracellular DEG could not be detected intracellularly after just 15 min of administration of the labelled compound (Extended Data Fig. 1f).

Glutarate is a product of tryptophan and lysine degradation, close to the terminus of the kynurenine pathway (Fig. 1e). Although a great deal is known about immunoregulatory aspects of other parts of the kynurenine pathway, there is only a very limited literature concerned with glutarate in immune cells. We thus sought to determine the amount of glutarate present in naive and activated CD8⁺ T cells. Mass spectrometry was used to determine intracellular levels of endogenous glutarate in CD8⁺ T cells: we found that glutarate levels increased substantially after T cell activation (Fig. 1f). These activation-induced increases in intracellular glutarate correlate with previously published decreases in GCDH protein copy numbers after T cell activation (Fig. 1g)³⁰.

Glutarate levels in activated T cells are significantly higher than, for example, the intracellular levels of succinate, a known immunometabolite (Extended Data Fig. 1h). Using previously published CD8⁺ T cell volumes, we determined that the approximate concentration of glutarate is 0.6 mM in activated CD8⁺ T cells¹¹. Treating CD8⁺ T cells with 500 μM DEG for 7 days increased measured intracellular glutarate concentrations by approximately twofold (Extended Data Fig. 1i).

T cell metabolism is greatly altered by T cell activation; a major driver of this metabolic change is the hypoxia-inducible factor 1- α (HIF-1 α) transcription factor. HIF-1 α is stabilized after CD8⁺ T cell activation even when T cells are cultured at high oxygen levels³¹, and the accumulation of a number of immunometabolites are affected by HIF-1 α levels. To determine if the observed increase of glutarate levels after T cell activation was HIF-1-dependent, we assayed glutarate levels in HIF-1 α proficient and HIF-1 α null (HIF-1 knockout) mouse CD8⁺ T cells and found that the activation-induced increases in glutarate seen in wild-type (WT) cells is almost completely absent in HIF-1 knockout cells (Fig. 1h). This finding indicates that the HIF-1 α transcription factor is essential for modulating T cell glutarate levels. We also found that culturing T cells at 1% oxygen for 24 h increased glutarate levels approximately twofold compared to culturing T cells at 21% oxygen levels (Fig. 1i). Consistent with this finding, we found that *GCDH* gene expression levels are decreased in T cells transfected with HIF-1 α -overexpressing, but not HIF-2 α -overexpressing T retroviral vectors (Fig. 1j and Extended Data Fig. 1j)³².

Given that expression of the *GCDH* encoding gene and GCDH protein levels fluctuate in CD8⁺ T cells, and that these variations correlate with changes in intracellular glutarate levels, we wished to determine the extent to which genetically modifying GCDH might influence CD8⁺ T cell phenotype by altering endogenous glutarate levels in CD8⁺ T cells. For these experiments, we undertook both silencing of GCDH (shGCDH) and overexpression of GCDH (GCDH overexpressed) with, respectively, transfection of either short hairpin RNA (shRNA) or overexpression vectors (Extended Data Fig. 1k,l). The shGCDH vector caused reduced GCDH protein levels and the GCDH overexpressed vector caused increased GCDH protein levels in T cells after transduction (Extended Data Fig. 1k,l). The shGCDH vector increased endogenous glutarate levels in HEK cells transduced with it; there were decreased levels of glutarate found in HEK cells overexpressing GCDH (Extended Data Fig. 1m). The overexpression of GCDH even reduced the elevated levels of glutarate in DEG-treated HEK cells (Extended Data Fig. 1n). Thus, these vectors enabled us to query the role of endogenous intracellular glutarate.

We found that both CD8⁺ T cells treated with DEG and CD8⁺ T cells treated with shGCDH, showed similar increases in expression of the cytotoxic effector molecule granzyme B (GZMB) (Fig. 1k). Following on from our observations that DEG alters T cell differentiation, we examined multiple exhaustion-associated markers in treated cells and found that TOX, a transcription factor known to orchestrate exhaustion^{33,34}, and the exhaustion markers TIM3 and LAG3, were all downregulated in human CD8⁺ T cell cultures after 10 days of DEG treatment (Fig. 1k). In contrast, reducing glutarate levels via overexpression of GCDH (with the GCDH overexpressed vector) resulted in increased expression of

TOX, TIM3 and LAG3. Supplementing GCDH-overexpressed CD8⁺ T cells with DEG counteracted the effects of GCDH overexpression on TIM3 and LAG3 (Fig. 1k). Taken together, these data illustrate that glutarate can alter CD8⁺ T cell differentiation.

Glutarate is an inhibitor of α KGDDs

Glutarate has structural similarities to 2HG, fumarate, succinate and α KG, and thus is a candidate competitive inhibitor of α KGDDs^{14–18}. To determine whether this was in fact the case, we focused on three subfamilies of the most intensively studied α KGDDs: the DNA-demethylating Ten-eleven translocation methylcytosine dioxygenases (TETs), the HIF prolyl 4-hydroxylases (HIF-P4Hs) and the histone lysine demethylases (KDMs). All of these enzymatic reactions are depicted in Extended Data Fig. 2a.

In cell-free enzymatic activity assays, glutarate inhibited recombinant TET2 with a half maximal inhibitory concentration (IC₅₀) of 1.5 mM (Fig. 2a, left). This inhibition is competitive with α KG, as indicated by reduced inhibition with increased levels of α KG (Fig. 2a, right). Competitive inhibition of TET2 correlated with an observed decrease in 5hmC (the reaction product of TET2) levels in a dose-dependent manner in human CD8⁺ T cells cultured with DEG for 7 days (Fig. 2b). DEG did not inhibit TET2 in cell-free assays (Extended Data Fig. 2b), providing further evidence that our observed results are due to free glutarate.

Glutarate also inhibited the HIF-prolyl4hydroxylase-1 (HIF-P4H-1) enzyme in vitro, with an IC₅₀ of 2 mM in a cell-free assay (Fig. 2c). To test HIF-P4H inhibition via DEG treatment in a cellular system, we used a luciferase reporter assay driven by a Gal4 response element (GRE-luc), pFLAG-Gal4-mHIF-1 α N-terminal transcription activation domain (NTAD)³⁵. The NTAD contains proline residues that are hydroxylated by HIF-P4H enzymes to target the protein for degradation; thus, luciferase expression in this assay is controlled by HIF-P4H hydroxylation activity against the pFLAG-Gal4-mHIF-1 α NTAD. We found that DEG can inhibit cellular HIF-P4H activity in this model system (Fig. 2d). HIF-P4H-1 inhibition by glutarate was reduced when increasing concentrations of α KG were added to the culture (Fig. 2e), indicating that, as with TET2 inhibition, glutarate inhibits HIF-P4H-1 in an α KG-competitive manner. This inhibition of HIF-P4H-1 was correlated with increased expression of several HIF target genes in DEG-treated CD8⁺ T cells for 7 days (Extended Data Fig. 2c).

To determine if glutarate also inhibits KDM enzymes, we cultured CD8⁺ T cells with DEG for 7 days and determined the methylation status of a number of histone 3 (H3) lysine residues (Fig. 2f). DEG treatment of CD8⁺ T cells increased dimethylation and trimethylation of H3K9 and trimethylation of H3K27 (Fig. 2f). This increase in H3K9 and H3K27 trimethylation was abrogated by the addition of equimolar amounts of α KG (Figs. 2g,h), while H3K9me2 levels were not reduced with the

Fig. 1 | Glutarate is an endogenous regulator of CD8⁺ T cell function.

a,b, Percentage of CD62L^{hi}CD44^{hi} (**a**) and number of total murine CD8⁺ T cells (**b**) after 7 days of treatment with 400 μ M of test compound. Ordinary one-way analysis of variance (ANOVA) relative to untreated control cells (Ctl); $n = 4$. **c**, Representative flow cytometry counter of mouse and human CD8⁺ T cells treated with or without 500 μ M DEG for 7 days. Grey (left), Ctl; blue (right), DEG 500 μ M. **d**, Heatmap representing the proportion of mouse CD8⁺ T cells expressing CD62L/CD44 (left) and the proportion of human CD8⁺ T cells expressing CCR7/CD45RO (right) after 7 days of treatment with increasing concentrations of DEG. Two-way ANOVA relative to Ctl; $n = 4–5$. **e**, Pathway of lysine and tryptophan catabolism (adapted from BioRender.com). **f**, Glutarate levels in naive and 72-h activated mouse CD8⁺ T cells. Two-tailed paired t -test; $n = 3$. **g**, GCDH protein copy number in naive or activated CD8⁺ T cells from P14 transgenic mice. Two-tailed unpaired t -test; $n = 3$. Data from the ImmPres database³⁰. **h**, Glutarate levels in naive or 72-h activated CD8⁺ T cells isolated from Hif-1 α ^{loxP/loxP} or Hif-1 α ^{loxP/loxP} dlck^{Cre} mice (HIF knockout). Two-way ANOVA; $n = 3$. **i**, Glutarate levels in mouse CD8⁺ T cells cultured at 21% or 1% oxygen for 24 h from day 5 after activation. Two-tailed paired t -test; $n = 3$. **j**, GCDH gene counts

per million (CPM) in HIF-1-overexpressing mouse CD8⁺ T cells. Two-tailed unpaired t -test; $n = 3$ ³². **k**, Expression of markers of T cell differentiation and exhaustion in human CD8⁺ T cells after 7–10 days of treatment with or without DEG 500 μ M or transduction with either shGCDH or GCDH-overexpressing vector. Expression was determined by flow cytometry and is shown as the mean fluorescence intensity (MFI) fold change relative to the untreated control (black dashed line). Two-tailed, one-sample Wilcoxon rank-sum test and ordinary one-way ANOVA. (GZMB DEG 500 μ M, $n = 13$; GZMB shGCDH, $n = 11$; GZMB GCDH overexpressed, $n = 11$; GZMB GCDH overexpressed + DEG 500 μ M, $n = 5$; TOX DEG 500 μ M, $n = 11$; TOX shGCDH, $n = 11$; TOX GCDH overexpressed, $n = 11$; TOX GCDH overexpressed + DEG 500 μ M, $n = 5$; TIM3 DEG 500 μ M, $n = 16$; TIM3 shGCDH, $n = 6$; TIM3 GCDH overexpressed, $n = 12$; TIM3 GCDH overexpressed + DEG 500 μ M, $n = 6$; LAG3 DEG 500 μ M, $n = 12$; LAG3 shGCDH, $n = 11$; LAG3 GCDH overexpressed, $n = 11$; LAG3 GCDH overexpressed + DEG 500 μ M, $n = 6$). All scatter plots show the median + the 95% confidence interval (CI), where each dot represents one donor (murine or human as indicated). * $P < 0.05$, ** $P < 0.01$, *** $P < 0.001$, **** $P < 0.0001$.

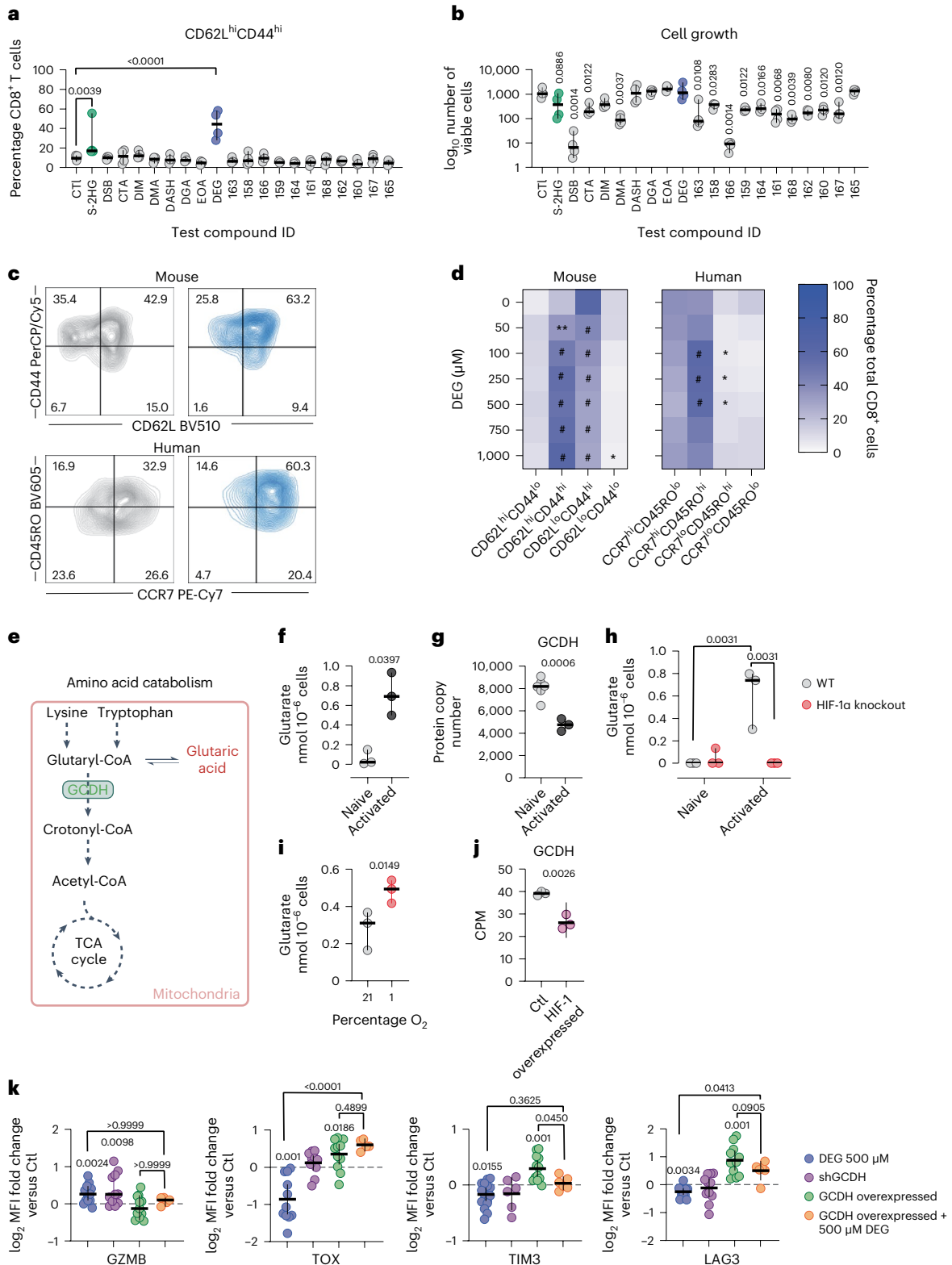
addition of α KG (Extended Data Fig. 2d). As KDM4C and KDM6A are responsible for the demethylation of H3K9me3 and H3K27me3, respectively, we performed cell-free enzymatic activity assays with these enzymes and found that glutarate inhibited KDM4C with an IC_{50} of 1 mM and KDM6A with an IC_{50} of 0.6 mM (Figs. 2i,j). As expected, DEG alone was not capable of inhibiting KDM4C activity in a cell-free assay (Extended Data Fig. 2e).

These data indicate that glutarate is an inhibitor of at least three specific α KGDDs, namely, the TET2, HIF-P4H-1 and KDM4C/6A

enzymes. This inhibition correlates with multiple changes to cellular gene expression and epigenetic profiles, including specific HIF targets, increased histone methylation and decreased DNA demethylation.

Glutarylation of PDH disrupts lipoylation

Glutarylation, a recently discovered post-translational modification (PTM), uses glutarate in its CoA form, glutaryl-CoA, as a substrate. The reaction can occur both enzymatically and non-enzymatically, while deglutarylation is thought to be mediated by SIRT5 (refs. 36–38)



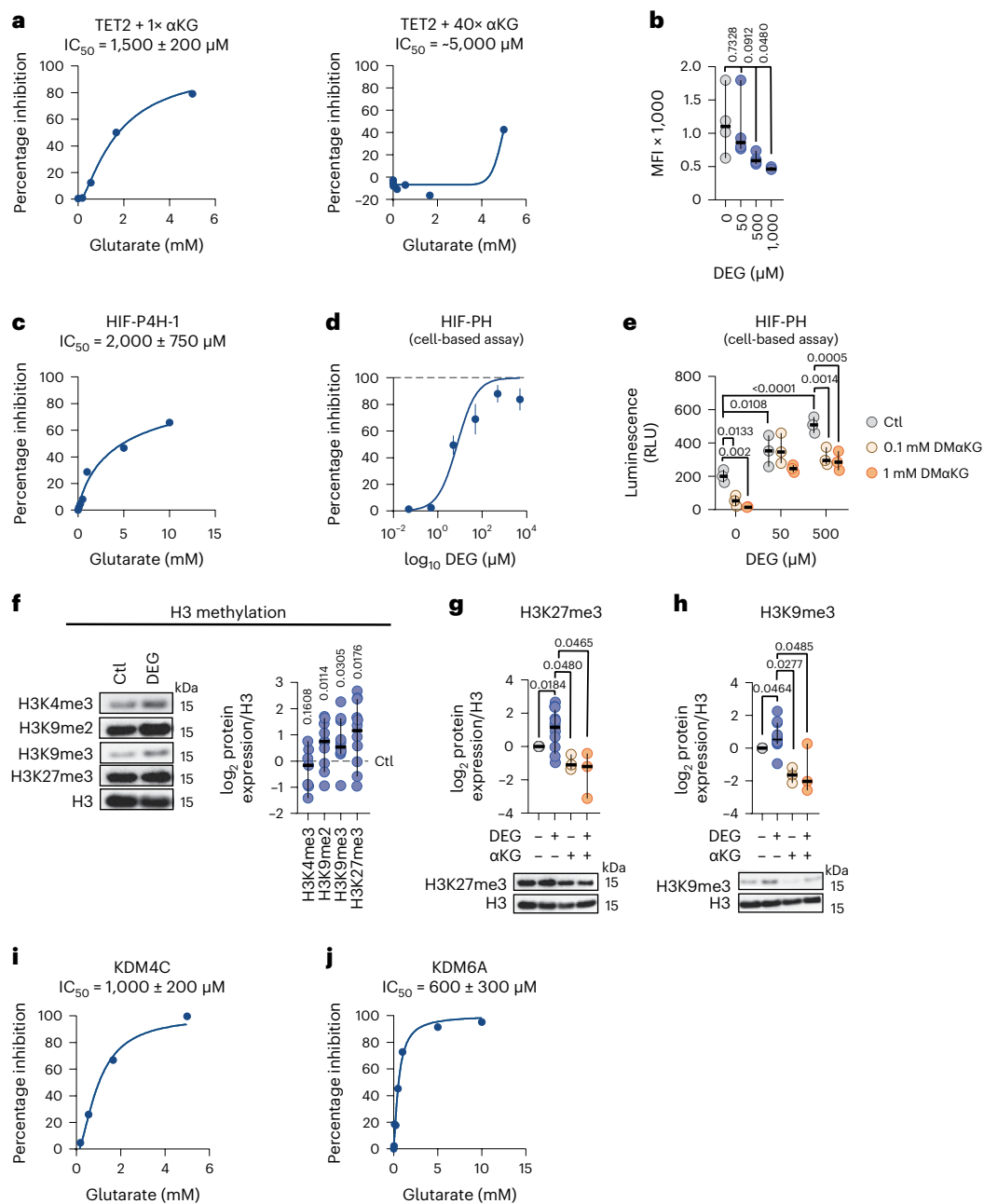


Fig. 2 | Glutarate is an inhibitor of αKG-dependent reactions. **a**, Cell-free enzymatic inhibition assay for TET2 using increasing concentrations of glutarate, using 1× IC₅₀ for αKG (left) or 40× IC₅₀ for αKG (right). **b**, 5hmC MFI, as determined using flow cytometry, in human CD8⁺ T cells after 7 days of treatment with increasing concentrations of DEG. Ordinary one-way ANOVA; $n = 4$. **c**, Cell-free enzymatic inhibition assay for HIF-P4H-1 using increasing concentrations of glutarate. **d**, HIF-PH activity luciferase reporter assay in mouse embryonic fibroblasts (MEFs) treated for 16 h with increasing concentrations of DEG. Data points are the mean ± s.e.m. $n = 9$. **e**, HIF-PH activity luciferase reporter assay in MEFs treated for 16 h with DEG and dimethyl αKG (DMαKG). Two-way ANOVA; $n = 3$. RLU, relative light unit. **f**, Representative western blot and log₂ fold change in protein expression of specific histone 3 (H3) methylation sites in human CD8⁺ T cells treated for 7 days with or without DEG 500 μM. Each dot represents one human donor normalized to total H3 and relative to untreated control (dashed

black line). Two-sided, one-sample *t*-test; H3K4me3, $n = 6$; H3K9me2, $n = 11$; H3K9me3, $n = 11$; H3K27me3, $n = 10$. **g**, Representative western blots and log₂ fold change protein expression of H3K27me3 in human CD8⁺ T cells treated with or without 500 μM DEG or 500 μM αKG for 7 days. Ordinary one-way ANOVA; DEG, $n = 10$; αKG, $n = 3$; αKG + DEG, $n = 3$. **h**, Representative western blots and log₂ fold change protein expression of H3K9me3 in human CD8⁺ T cells treated with or without 500 μM DEG or 500 μM αKG for 7 days. Ordinary one-way ANOVA; $n = 3$ –5. DEG, $n = 11$; αKG, $n = 3$; αKG + DEG, $n = 3$. **i**, Cell-free enzymatic inhibition assay for KDM4C using increasing concentrations of glutarate. **j**, Cell-free enzymatic inhibition assay for KDM6A using increasing concentrations of glutarate. Cell-free enzymatic assay graphs showing Michaelis–Menten line of best fit of at least three independent experiments. All scatter plots show the median + 95% CI, where each dot represents one donor as indicated. * $P < 0.05$, ** $P < 0.01$, *** $P < 0.001$, **** $P < 0.0001$.

(Fig. 3a). Recently, studies of mouse liver and brain showed that glutarylation can modify a range of proteins^{36,39}. Given our observation of fluctuating levels of glutarate in CD8⁺ T cells (Fig. 1f,i), we wished to determine whether glutarylation also takes place in CD8⁺ T cells.

We determined this first by undertaking whole-protein lysate western blot analyses with a pan-lysine glutarylation (K-glutarylation) antibody^{36,38}. We found that protein glutarylation is clearly detectable in CD8⁺ T cells (Fig. 3b). We also found that glutarylation patterns

change strikingly after CD8⁺ T cell activation (Fig. 3b). Glutarylation patterns were also altered when cells were exposed to different oxygen tensions (Fig. 3c and Extended Data Fig. 3a) and when treated with DEG (Fig. 3d and Extended Data Fig. 3b). Interestingly, shifts in glutarylation could be detected after just 30 min of culture with DEG (Fig. 3e and Extended Data Fig. 3c). Since, as shown in Extended Data Fig. 1g, DEG is converted within 15 min to glutarate intracellularly, it is likely that the DEG-induced glutarylation observed after 30 min of DEG treatment is a direct result of increases in intracellular glutarate.

In these western blot assays we observed a relatively small number of proteins with marked changes in glutarylation caused by T cell activation (Fig. 3b–e). One notable protein in this assay was a protein of approximately 70 kDa. This protein was also the moiety most affected by hypoxia and by exposure of T cells to DEG (Extended Data Fig. 3a–c). To establish the identity of this and other glutarylated proteins in CD8⁺ T cells, we performed an immunoprecipitation (IP) assay with a K-glutarylation antibody (Fig. 3f). We then excised the observed bands and used mass spectrometry in conjunction with the SwissProt protein database to identify them (Extended Data Fig. 3d). Proteins with the highest posterior error probability (PEP) score in each band are listed in Extended Data Fig. 3e.

Three non-cytoskeletal/histone proteins were positively identified; (1) 2-oxoglutarate dehydrogenase (OGDH); (2) dihydrolipoyl lysine residue acetyltransferase (DLAT) (also known as the E2 subunit of the PDHc (PDHE2)); and (3) PDHE1 component subunit beta (PDHE1β) (Extended Data Fig. 3e). Glutarylation targets were confirmed by reverse IP, in which an IP with the target antibody was performed and then the resulting western blot was probed with the K-glutarylation antibody.

IP and subsequent western blot analysis of the PDHc (which includes PDHE2 and PDHE1β) revealed that it was the PDHE2 subunit alone that in our assays was clearly and detectably glutarylated (Fig. 3g,h). IP and subsequent western blot analysis with the K-glutarylation antibody revealed that OGDH is not detectably glutarylated in this system (Extended Data Fig. 3f,g). Thus, the PDHE2 subunit (67 kDa) was the only glutarylation target identified both by mass spectrometry and subsequently confirmed by reverse IP.

PDHc catalyses the conversion of pyruvate to acetyl-CoA and thus links glycolysis and the tricarboxylic acid (TCA) cycle⁴⁰. PDHc consists of multiple copies of three catalytic enzymes: PDH (E1); dihydrolipoamide acetyltransferase (PDHE2); and dihydrolipoamide dehydrogenase (DLD) (E3) (Fig. 3i). The E2 subunit is the functional core of the PDHc and provides catalytic activity via cyclical reduction and oxidation of its lipoyl domains, channelling substrates between individual enzymes' active sites in the PDHc. The multidomain E2 subunit consists of the C-terminal catalytic domain, the peripheral subunit-binding domain and the N-terminal ends of 1–3 lipoyl domains^{41–44}. The lipoyl domains contain one lipoic acid covalently attached to a lysine residue; this lipoic acid is essential for PDHc catalytic activity⁴⁵.

Following the observation that lysine residues of PDHE2 can be glutarylated, we sought to determine if lysine glutarylation was disrupting lipoic acid conjugation to PDHE2 lysine residues, thereby

disrupting normal PDHc functioning. We treated human CD8⁺ T cells with DEG and observed reduced PDHE2 lipoyl level (Fig. 3j,k). Proteomic analysis of PDHE2 immunoprecipitated from HeLa cells revealed that DEG treatment reduced the levels of lipoyl K259, while increasing glutaryl-lipoyl K259 (Fig. 3l and Extended Data Fig. 3h). In addition to the observed glutarylation site on K259, two additional PDHE2 lysine residues were found by proteomics to have glutaryl groups attached, that is, K396 and K482.

These data illustrate that glutarylation occurs in CD8⁺ T cells, that this glutarylation status changes after activation, and identifies PDHE2 as a glutarylation target, while providing evidence that glutarylation disrupts normal PDHc lipoylation, potentially altering the catalytic activity of the complex.

Glutarate modulates metabolic state

PDHc links glycolysis to the TCA cycle as noted above; thus, we hypothesized that glutarylation might decrease PDHc enzymatic activity, with a resultant increased glycolytic rate. To test this, we performed a direct enzymatic activity assay of the PDHc on CD8⁺ T cell lysates and found that both acute (30 min) and chronic (seven day) exposure to DEG resulted in decreased PDHc activity (Fig. 4a). Reduced PDHc activity was also observed in CD8⁺ T cells with partially silenced GCDH, and thus increased endogenous glutarate levels (Extended Data Fig. 4a). As expected, this reduction in PDHc activity resulted in increases in the basal extracellular acidification rate (ECAR) (Fig. 4b), as pyruvate was metabolized by the lactate dehydrogenase enzyme to form lactate.

To explore further the metabolic consequences of this observed glutarate-induced reduction in PDHc activity, we performed a glycolysis stress test (GST). Acute effects were determined by treating CD8⁺ T cells with DEG for 30 min while plated in the Seahorse XF Analyzer. Chronic effects were determined by performing a standard GST in CD8⁺ T cells that had been cultured with DEG for 7 days before assay. Both acute and chronic exposure to DEG resulted in an increased glycolytic rate (Fig. 4c,d and Extended Data Fig. 4b,c).

Glycolysis is highly regulated by the HIF transcription factor, and because, as shown above, glutarate is a competitive inhibitor of HIF-P4H-1 (Fig. 2c–e) and thus can induce the transcription of HIF target genes (Extended Data Fig. 2c), we next sought to determine the relative contribution of glutarate-induced HIF activity to the observed metabolic changes we observed: reduced PDHc activity and increased glycolysis. Phosphorylation of PDHc by pyruvate dehydrogenase kinase (PDHK) is a known regulator of PDHc activity, and although DEG treatment of CD8⁺ T cells increased the mRNA levels of PDHK1 (Extended Data Fig. 2c), PDHK1 protein levels were not significantly altered after DEG treatment (Extended Data Fig. 4d). Importantly we did not observe any changes in PDHc phosphorylation levels after DEG treatment (Extended Data Fig. 4e). Additionally, DEG treatment did not alter the protein expression of the PDHc (Extended Data Fig. 4f).

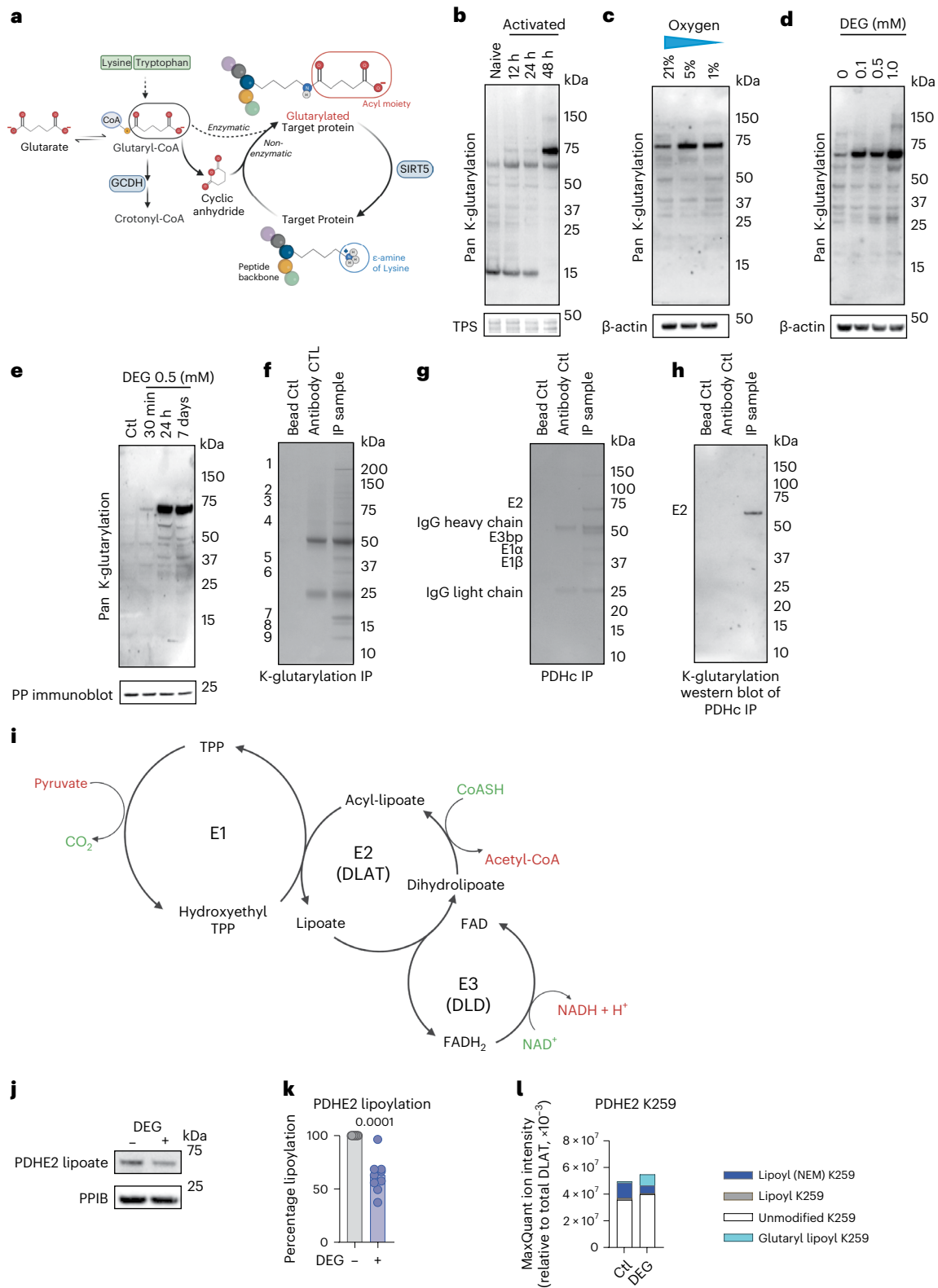
The glucose transporter GLUT1 is also a HIF-regulated gene, and so we also determined the rate of glucose uptake in cells treated with DEG. Again, we observed no changes, which is consistent with no HIF-induced functional effects (Extended Data Fig. 4g). Although

Fig. 3 | Glutarylation of PDH disrupts lipoylation. **a**, Model of protein lysine glutarylation (adapted from [BioRender.com](#)). **b**, Representative western blot of naive and activated human CD8⁺ T cells. *n* = 3. TPS, total protein stain. **c**, Representative western blot of activated human CD8⁺ T cells cultured at different oxygen tensions (21%, 5% or 1%). *n* = 3. **d**, Representative western blot of human CD8⁺ T cells cultured with increasing concentrations of DEG for 7 days. *n* = 4. **e**, Representative western blot of activated human CD8⁺ T cells cultured with 500 μM DEG for several different time lengths as indicated. All samples were collected 7 days after activation. *n* = 5. **f**, Representative Coomassie brilliant blue staining of proteins immunoprecipitated with a pan-K-glutarylation antibody and separated by SDS–polyacrylamide gel electrophoresis (PAGE). A total of 30 × 10⁶ mouse CD8⁺ T cells, 7 days after activation, were used. *n* = 3.

g, Representative Coomassie brilliant staining of immunoprecipitated PDHc separated by SDS–PAGE. A total of 30 × 10⁶ mouse CD8⁺ T cells, 7 days after activation, were used. *n* = 3. **h**, Representative K-glutarylation western blot of immunoprecipitated PDHc as described in Fig. 4g. *n* = 3. **i**, Schematic of the reactions catalysed by the individual subunits of the PDHc (adapted from [BioRender.com](#)). **j**, Representative western blot of PDHE2 lipoyl levels in human CD8⁺ T cells treated with 500 μM DEG for 24 h. *n* = 12. **k**, Percentage lipoylation calculated from Fig. 4k, where untreated control represents 100% lipoylation. Two-tailed, paired *t*-test; *n* = 12. **l**, Quantified proteomic analysis of select PTMs on PDHE2 K259, relative to total PDHE2, using HeLa cells treated with 500 μM DEG for 24 h.

as shown above, glutarate is a competitive inhibitor of HIF-P4H-1 (Fig. 2c–e), a more extended or higher exposure to glutarate than those found under our experimental conditions may be required to elicit a functional HIF response. Taken together, these data suggest that the key factor in the alteration of glycolytic rate in DEG-treated cells is glutarylation of PDHE2, and that it is this PTM of PDHE2 that is responsible for both altered PDHc activities in DEG-treated cells and the increases in ECAR and glycolytic rate observed after treatment.

Despite reduced PDHc activity, acetyl-CoA levels were not lower after in vitro treatment with DEG (Fig. 4e), indicating potential compensation from alternative pathways. Additionally, mitochondrial respiration, as characterized by cellular basal oxygen consumption rates (OCRs), was either maintained or increased after DEG exposure (Fig. 4f). Glutarate in its CoA form, glutaryl-CoA, can form crotonyl-CoA before being further metabolized to acetyl-CoA; so while glutaryl-CoA may reduce acetyl-CoA generation from pyruvate via glutarylation of



PDHE2, acetyl-CoA levels, and thus mitochondrial oxidation, can be maintained as glutarate and used as a direct fuel source (Fig. 4j). During a standard mitochondrial stress test (MST), the addition of carbonyl cyanide-*p*-trifluoromethoxyphenylhydrazone (FCCP), the mitochondrial uncoupling agent, did not have an effect on OCR in cells treated acutely with DEG (Fig. 4g), while cells that had been treated for 7 days with DEG before assay had a reduced maximal OCR (Fig. 4h), indicating that although glutarate can maintain OCR, it is not as efficient as glucose in facilitating mitochondrial oxidation.

To better understand the consequences of providing glutarate as a fuel for mitochondrial oxidation, we measured cellular oxygen consumption while inhibiting, in different combinations, fatty acid, glucose and glutamine oxidation, the three main fuel sources for mitochondrial oxidation (Extended Data Fig. 4i). This was achieved via injection of etomoxir, UK5099 and Bis-2-(5-phenylacetamido-1,3,4-thiadiazol-2-yl)ethyl sulphide (BPTES), respectively, in cells plated in a Seahorse XF Analyzer. We found that while DEG-treated cells are not more dependent on any of these pathways (Extended Data Fig. 4j,k), treated cells do have an increased capacity to oxidize both fatty acids (Fig. 4i) and glucose (Extended Data Fig. 4k) when other fuel sources are limited. Additionally, these cells have increased levels of fatty acid synthase (*FASN*), fatty acid binding protein (*FABP*) and carnitine palmitoyltransferase 1A (*CPT1A*) gene expression (Extended Data Fig. 4h), suggesting that acetyl-CoA formed from glutarate breakdown may be used to generate fats via fatty acid synthesis, and that these fats can be used when there is a depletion of other nutrients.

These data illustrate that glutarate levels can modulate CD8⁺ T cell metabolism.

Glutarate treatment in vivo acts to reduce tumour growth

The metabolism of CD8⁺ T cells is a critical aspect of their effector function⁴⁶. Given our observations, in addition to the recent observation that PDHc inhibition can increase CD8⁺ T cell cytotoxicity and increase immunotherapeutic efficacy⁴⁷, and the ongoing clinical trials using PDHc inhibitors for several cancers^{48,49}, we sought to determine the effects of DEG in tumour immunotherapy models.

To test this, after 7 days of culture in DEG-containing medium, antigen-specific cytotoxicity was first determined in both a human CAR T cell system derived from human donor CD8⁺ T cells, and a murine system using transgenic OT1 CD8⁺ T cells (Fig. 5a). After 7 days of culture with DEG, murine OT1 CD8⁺ T cells were more proficient at killing ovalbumin (OVA)-expressing B16F10-OVA cancer cells (Fig. 5b), while DEG-treated human CD19⁺ CAR T cells secreted more interferon- γ (IFN γ) and exhibited increased cytotoxicity against CD19⁺ Raji cells (Fig. 5c). DEG treatment did not affect the growth of either the human CD19⁺ CAR T cells or the murine OT1 T cells (Extended Data Fig. 5a,b) or cause any toxicity in the tumour cells themselves (Extended Data Fig. 5c,d).

To determine whether increased endogenous glutarate levels in CD8⁺ T cells also increases the cytotoxic efficacy of CD8⁺ T cells, we

created a human HER2 CAR T system containing an miRNA-embedded shRNA against GCDH (HER2 CAR T_shGCDH) (Fig. 5d). HER2 CAR T cells with a non-targeted control (NTC) (HER2 CAR T_shNTC) were used as a control. CD8⁺ T cells expressing HER2 CAR T_shGCDH had significantly increased cytotoxicity against target HER2⁺ SKOV3 ovarian cancer cells when compared to control HER2 CAR T_shNTC cells (Fig. 5e). Cell growth was not affected in shGCDH-expressing cells (Extended Data Fig. 5e).

We next performed in vivo tumour growth experiments in which mice with HER2⁺ SKOV3 tumours were treated with HER2 CAR T_shGCDH cells (Fig. 5f). Mice treated with HER2 CAR T_shGCDH cells had reduced rates of tumour growth in 6 of 11 mice compared to mice treated with HER2 CAR T_shNTC cells (Fig. 5g). However, we did not observe a difference in the overall survival of mice (Fig. 5h).

We next wished to determine whether direct administration of DEG to tumour-bearing mice would result in a slowing of tumour growth. DEG is non-toxic and is in fact approved by the European Union for use as a food additive⁵⁰. To determine whether it could be used therapeutically, we carried out an experiment in which mice with B16F10-OVA melanoma tumours were injected intraperitoneally with DEG every 48–72 h (Fig. 5i). This treatment regimen significantly slowed tumour growth and significantly increased survival of DEG-treated mice (Fig. 5j,k).

To determine the mechanisms underlying the reduced tumour growth we observed in vivo after DEG treatment, we again undertook treatment of B16F10-OVA tumour-bearing mice with DEG every 48–72 h as described above. Ten days after the start of DEG treatment, we collected peripheral blood, tumours, spleens and tumour-draining lymph nodes from the experimental animals. Single-cell suspensions were generated from each sample and the quantity of several immune cell populations was determined (Extended Data Fig. 5f,g). CD3⁺ T cells, CD4⁺ T cells, CD8⁺ T cells, B cells, neutrophils, natural killer cells, monocytes, dendritic cells and macrophages were assayed for, and this analysis revealed a significant increase in both peripheral blood CD8⁺ T cells and tumour-infiltrating CD8⁺ T cells in DEG-treated animals relative to controls (Fig. 5l,m). No changes in other immune populations were observed, apart from a slight decrease in circulating B cells (Extended Data Fig. 5g). The CD8⁺ T cell phenotypic changes observed with ex vivo treatment with DEG (Fig. 1) are not observed in tumour-infiltrating CD8⁺ T cells in DEG-treated mice (Extended Data Fig. 5). Analysis of tumour-infiltrating lymphocytes revealed no changes in the expression of memory-associated markers (CD62L and CD44) or exhaustion-associated markers (TIM3, PD1, LAG3, TOX) in CD4⁺ or CD8⁺ cells (Extended Data Fig. 5h,i). Phenotypic analysis of circulating CD8⁺ T cells in DEG-treated mice was not performed in this study. Future studies will perform detailed analysis of both circulating and tumour-infiltrating CD8⁺ T cells in tumour-bearing mice treated with DEG to fully elucidate the in vivo effects of DEG treatment.

Fig. 4 | Glutarate modulates mitochondrial function by inhibiting PDH.

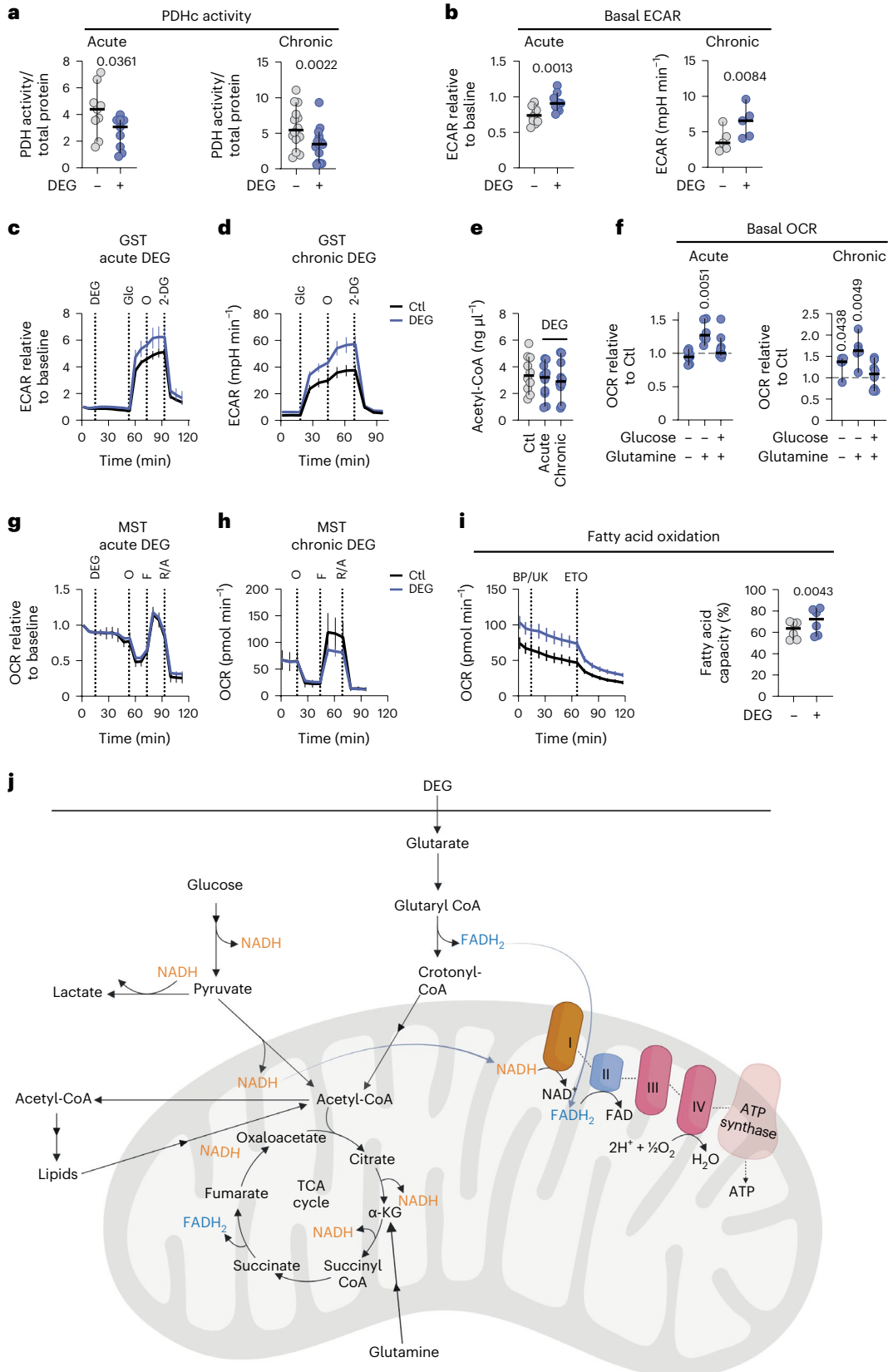
a, PDHc activity of CD8⁺ T cells treated with DEG for 30 min (acute) or 7 days (chronic), normalized to total protein concentration. Two-tailed, paired *t*-test; acute, *n* = 9; chronic, *n* = 14. **b**, Basal ECAR in CD8⁺ T cells as determined by Seahorse analysis after 30-min DEG treatment via Seahorse injection (acute, left) or after 7 days of in vitro culture with DEG (chronic, right). Acutely treated cells normalized to ECAR levels before DEG/Ctl injection. Two-tailed, paired *t*-test; acute, *n* = 10; chronic, *n* = 5. **c**, Seahorse analysis of ECAR levels in CD8⁺ T cells 7 days after activation. *n* = 10. **d**, Seahorse analysis of ECAR measurements during a standard GST of CD8⁺ T cells treated with or without DEG for 7 days. *n* = 6. **e**, Acetyl-CoA levels in CD8⁺ T cells treated with DEG for 30 min (acute) or 7 days (chronic). Repeated measures one-way ANOVA; *n* = 10. **f**, Basal OCR levels in CD8⁺ T cells as determined by Seahorse analysis after 30-min DEG treatment via Seahorse injection. During the assay, cells were plated in XF medium with or without glucose and glutamine as indicated. OCR is represented as the fold

change relative to untreated control. Two-tailed, one-sample *t*-test; acute, + glucose, – glutamine, *n* = 8; acute, – glucose, + glutamine, *n* = 6; acute, + glucose, + glutamine, *n* = 10; chronic, – glucose, – glutamine, *n* = 5; chronic, – glucose, + glutamine, *n* = 6; chronic, + glucose, + glutamine, *n* = 8. **g**, Seahorse analysis of OCR in CD8⁺ T cells (7 days after activation). *n* = 10. **h**, Seahorse analysis of OCR measurements during a standard GST of CD8⁺ T cells treated with or without DEG for 7 days as described in Extended Data Fig. 4i. Calculated percentage of fatty acid capacity (right): two-tailed, paired *t*-test; *n* = 6. **j**, Schematic illustrating the contribution of glutarate, glucose, lipids and glutamine to cellular metabolism (adapted from BioRender.com). All experiments shown used 500 μ M DEG. All scatter plots show the median + 95% CI, where each dot represents one human. The ECAR and OCR time course graphs show the mean and error with the 95% CI.

These data illustrate that glutarate can enhance CD8⁺ T cell cytotoxicity, and that *in vivo* treatment of tumour-bearing mice with an esterified form of glutarate can reduce tumour growth and increase animal survival, highlighting the use of this immunometabolite as a potential cancer therapy.

Discussion

The intrinsic link between metabolism and cellular function was first highlighted by the discovery of mutations in genes encoding metabolic enzymes. Mutations in fumarate hydratase, succinate dehydrogenase and isocitrate dehydrogenase, all of which are key enzymes of the TCA



cycle, lead to the accumulation of fumarate, succinate and 2HG, respectively. At high levels, each of these metabolites can act as disease-driving signalling molecules.

Mutations in the GCDH enzyme can also be pathological and detrimental to normal development²⁶. There is also at least one report indicating that an unusual occurrence of glioblastoma has been found in patients with mutations in *GCDH*²¹. However, to date, the functions of glutarate have been almost exclusively studied in the context of patients and animal models of GA1. We showed that glutarate is present in CD8⁺ T cells and that its levels are influenced by both activation and oxygen status. We demonstrated that glutarate has an unexpected role in the regulation of cell physiology, particularly in the differentiation and metabolism of T cells. By acting as an inhibitor of α KGDDs, glutarate alters the transcriptional and epigenetic landscape of cells via inhibition of HIF-P4H and KDMs/TETs, respectively. We used CD8⁺ T cells as a model system, but note that glutarate has this inhibitory property both in cell-free assays and in a range of other cell types; thus, these effects are probably not exclusive to CD8⁺ T cells.

By altering glutarate levels in CD8⁺ T cells, either by supplementation with esterified glutarate, or by genetic manipulation of GCDH, we showed that in vitro glutarate promotes T_{CM} cell development and reduces expression of T cell exhaustion markers, while increasing cytotoxic function. Although in vivo treatment of tumour-bearing mice with DEG reduces tumour growth, while increasing the quantity of both circulating and tumour-infiltrating CD8⁺ T cells, the CD8⁺ phenotypic changes observed with ex vivo treatment with DEG were not observed in tumour-infiltrating CD8⁺ T cells. In an immune cell context, loss of TET2 expression promotes differentiation of CD8⁺ T cells into T_{CM} cells⁵² and a disrupted *TET2* gene can promote the therapeutic efficacy of CAR T cells⁵³. We have illustrated that glutarate treatment of CD8⁺ T cells results in direct TET2 inhibition, correlating with both the increased levels of T_{CM} populations we see in activated CD8⁺ T cells and an increased killing of target cells.

CD8⁺ T cell differentiation from a naive quiescent cell to an effector or memory cell requires dynamic epigenetic remodelling, resulting in altered gene accessibility profiles⁵⁴. H3K9me3 and H3K27me3 are known repressive histone modifications and are both increased in activated CD8⁺ T cells cultured with DEG, after direct competitive inhibition of KDM4C and KDM6A, respectively. H3K27me3 expression is reduced after T cell activation⁵ and in vivo studies have shown that its levels are highest in T_{CM} and naive CD8⁺ T cells¹¹. In this study, we illustrated that, similarly to the effects seen after exposure to S-2HG¹¹, DEG facilitates retention of H3K27me3, a marker correlated with T_{CM} cell development. Glutarate additionally inhibits the HIF prolyl hydroxylase HIF-P4H-1, albeit with a much higher IC₅₀ than observed for the KDM and TET2 enzymes. Our findings indicate that glutarate is a competitive inhibitor of α KGDDs and this should be considered as a likely aspect of GA1 pathology, given the high levels of intracellular glutarate seen in that disease.

In this study, we showed that the E2 subunit of PDHc is a major target of glutarylation in CD8⁺ T cells. Glutarate in its CoA form, that is, glutaryl-CoA, acts as a substrate for glutarylation³⁶. Glutarylation has important roles in mitochondrial dynamics, antioxidant defence, sperm motility, lysine oxidation and apoptotic signalling^{39,55–58}. One recent study found that GCDH knockdown in melanoma resulted in programmed cell death via glutarylation of NRF2 (ref. 55). We did not find any evidence for increased cell death after GCDH silencing or increased glutarylation via DEG treatment in CD8⁺ T cells or in any of the other cell types that we examined in this study.

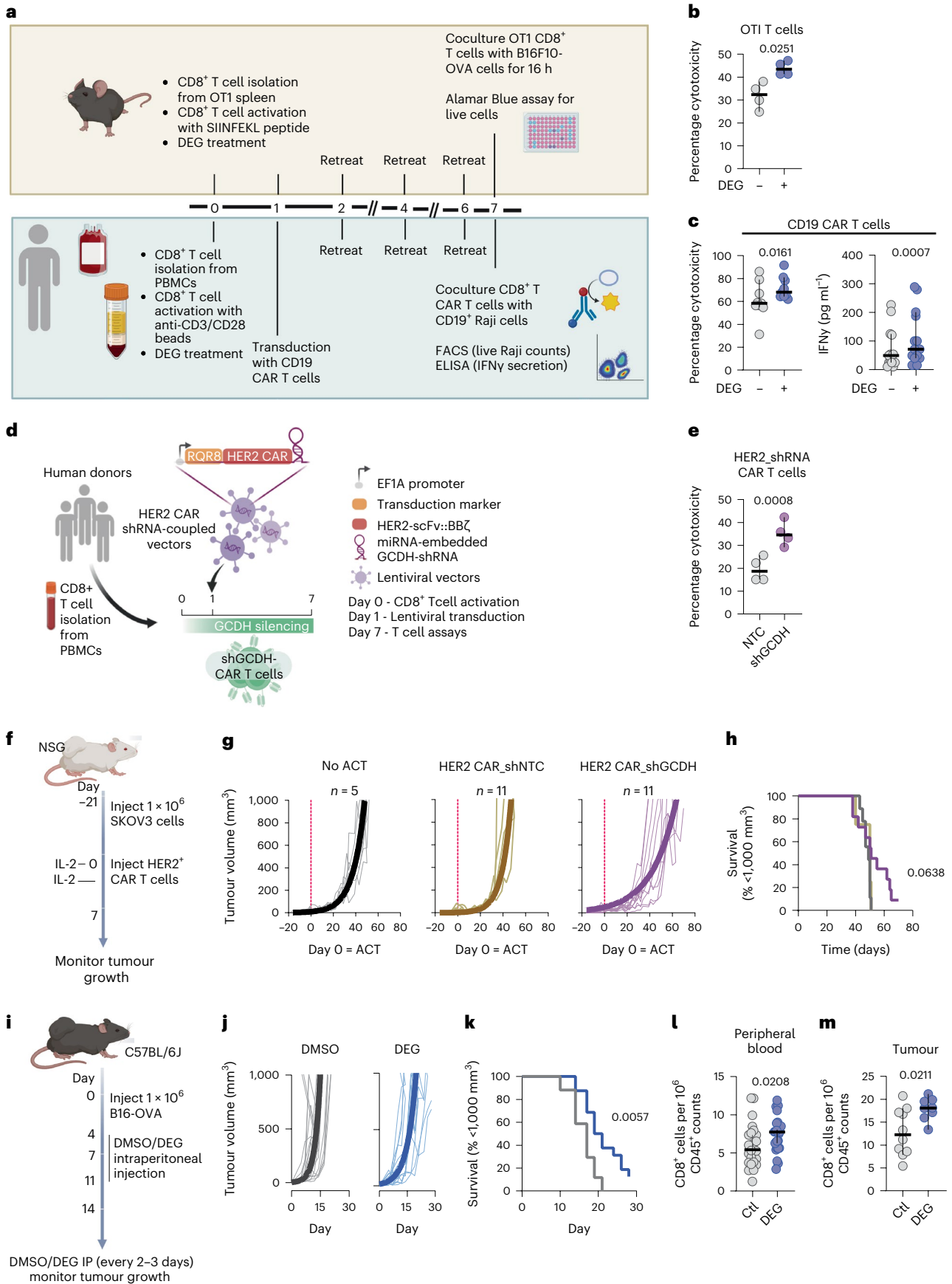
In this study, we provide evidence that lysine glutarylation of the E2 subunit of PDHc disrupts normal lipoylation, resulting in altered PDHc activity, which correlates with increased pyruvate conversion to lactate and increased glycolysis. This reaction occurs rapidly in cells treated with diethyl glutarate. Although inhibition of HIF-P4H-1 induces the transcription of genes associated with glycolysis, the levels of glutarate used in this study did not result in increased protein expression of PDHK1, an increased PDHE1 phosphorylation or in an increased glucose uptake; this indicates that the increase in glycolytic capacity and ECAR observed in this study are probably, for the most part, independent of HIF-P4H-1 inhibition. This indicates that glutarylation represents a mechanism for PDHc control, acting via disruption of lipoylation, and demonstrates the importance of lipoate modifications in controlling the activity of PDHc^{59–61}.

Constant regeneration of acetyl-CoA is essential for cells to maintain oxidative phosphorylation. Although glutarate reduces PDHc activity via glutarylation, cells treated with glutarate do not have a reduced acetyl-CoA pool, probably owing to compensation from glutarate breakdown and fatty acid oxidation. This results in maintenance of mitochondrial oxidative phosphorylation despite the reduced PDHc activity caused by glutarylation of PDHE2. The breakdown of glutarate to crotonyl-CoA, and subsequently to acetyl-CoA, generates FADH₂, as opposed to acetyl-CoA formation from pyruvate, which generates NADH. NADH is a stronger reducing agent and enters the electron transport chain (ETC) at complex I, in contrast to FADH₂, which enters the ETC at complex II. This differential contribution to mitochondrial membrane potential results in a reduced maximal OCR on addition of FCCP to glutarate-treated cells, indicating that, while glutarate can be used as an alternative fuel source for mitochondrial oxidation, it is not as efficient as glucose itself.

In this study, we revealed a potentially central role for glutarate as a modulator and regulator of CD8⁺ T cell metabolism and cytotoxicity. We illustrated that glutarate can influence CD8⁺ T cell differentiation and increase effector function. We showed that glutarate is an inhibitor of α KGDDs, which has many implications for better understanding the epigenetic and transcriptional landscape of cells in a catabolic state. We additionally showed that PDHE2 is a direct target of glutarate-mediated glutarylation and is involved in the control of this crucial metabolic complex. Finally, we highlighted the potential use of

Fig. 5 | Glutarate reduces tumour growth and increases CD8⁺ T cell numbers and tumour infiltration. **a**, Model of in vitro cytotoxicity assays; 500 μ M DEG was used (adapted from BioRender.com). ELISA, enzyme-linked immunosorbent assay; FACS, fluorescence-activated cell sorting. **b**, Percentage cytotoxicity of OT1 cells after coculture with B16F10-OVA cells as described in **a**. Two-tailed, paired *t*-test; *n* = 4. **c**, Percentage cytotoxicity (left) and IFN γ expression (right) of CD19 CAR T cells after coculture with CD19⁺ Raji cells as described in **a**. Two-tailed, paired *t*-test; cytotoxicity, *n* = 9; IFN γ , *n* = 14. **d**, Model of HER2 CAR T shRNA cell generation (adapted from BioRender.com). **e**, Percentage cytotoxicity of HER2 CAR T cells with embedded shGCDH or shNTC as determined by Alamar Blue assay after coculture with HER2-expressing SKOV3 cells. Two-tailed, paired *t*-test; *n* = 4. **f**, Adoptive cell therapy (ACT) model with CAR T cells. Tumour growth was monitored every 2–3 days until day 70. **g**, Tumour growth data. The thin lines represent tumour growth from individual mice and the thick lines represent an exponential (Malthusian) growth curve. **h**, Survival curves using

1,000 mm³ tumour volume as the threshold. log-rank (Mantel–Cox) test. **i**, Tumour growth model; 1.0 \times 10⁶ B16F10-OVA cells were injected subcutaneously into C57BL/6j mice. From day 4 after tumour inoculation, mice were injected interperitoneally with 10 mg kg⁻¹ DEG or dimethyl sulfoxide (DMSO) Ctl every 2–3 days. On day 14 after tumour inoculation, peripheral blood, tumour, spleen and tumour-draining lymph node from some mice were processed to single-cell suspensions and analysed by flow cytometry. Tumour growth was monitored until day 30. **j**, Tumour growth data. The thin lines represent tumour growth from individual mice and the thick lines represent an exponential (Malthusian) growth curve. **k**, Survival curves using 1,000 mm³ tumour volume as the threshold. log-rank (Mantel–Cox) test; *n* = 14. **l**, Frequency of CD8⁺ T cells in peripheral blood 14 days after tumour inoculation. Two-tailed *t*-test; *n* = 25. **m**, Frequency of CD8⁺ T cells in the tumours 14 days after tumour inoculation. Two-tailed, *t*-test; Ctl, *n* = 10; DEG, *n* = 8. All scatter plots show the median and 95% CI, where each dot represents one donor (human or murine as indicated).



glutarate administration in an immunotherapeutic model, illustrating the translational potential of these findings.

Methods

All animal experiments were performed in accordance with the ethical regulation of the UK Home Office and the University of Cambridge or the regional animal ethics committee of northern Stockholm, Sweden.

Human peripheral blood mononuclear cells (PBMCs) were obtained from the National Health Service (NHS) Blood and Transplant (NHSBT) (Addenbrooke's Hospital, Cambridge, UK) or Karolinska Hospital Service, Sweden. Ethical approval was obtained from the East of England-Cambridge Central Research Ethics Committee (06/Q0108/281) and consent was obtained from all participants.

Mice

C57BL/6J mice (strain 632, Charles River Laboratories), were used in the in vitro assays and in the orthotopic tumour growth and infiltration experiments (male and female mice were 8–12 weeks old). NOD.Cg-Prkdc^{scid}/Il2rg^{tm1Wjl}/SzJ (NSG) mice (strain 005557, The Jackson Laboratory) were used in human CAR T cell experiments. Donor T cell receptor (TCR)-transgenic OT1 mice (003831, The Jackson Laboratory) were crossed with mice bearing the CD45.1 congenic marker (strain 002014, The Jackson Laboratory). Targeted deletion of HIF-1 in T cells was achieved by crossing homozygous mice carrying *loxP*-flanked *Hif1* alleles⁶² into a mouse strain of Cre recombinase expression driven by the distal promoter of the lymphocyte-specific *Lck* gene (strain 012837, The Jackson Laboratory). All experiments were performed with age-matched and sex-matched Cre-negative controls. TCR-transgenic OT1 mice and mice with targeted deletion of *Hif1* in T cells were bred and housed in specific pathogen-free conditions in accordance with the regional animal ethics committee of northern Stockholm, Sweden. All animal experiments were performed in accordance with the ethical regulation of the UK Home Office and the University of Cambridge or the regional animal ethics committee of northern Stockholm, Sweden.

Cell lines

B16F10 cells were originally purchased from ATCC (catalogue no. CRL-6475) and genetically modified to express OVA, enhanced green fluorescent protein (GFP) and neomycin phosphotransferase³². The resulting OVA expression B16F10-OVA cells were cultured in DMEM (catalogue no. 11995065, Thermo Fisher Scientific) containing 0.75 mg ml⁻¹ G418 sulphate (catalogue no. 10131027, Thermo Fisher Scientific). HEK 293T cells were purchased from Takara Bio (catalogue no. 632180) and cultured in DMEM. SKOV3 was purchased from ATCC (catalogue no. HTB-77) and cultured in McCoy's 5A (Modified) Medium (catalogue no. 16600082, Thermo Fisher Scientific). Raji-GFP-Luc cells were purchased from Biocytogen (catalogue no. B-HCL-010) and cultured in Roswell Park Memorial Institute (RPMI) 1640 (catalogue no. 21875, Thermo Fisher Scientific). Jurkat cells were purchased from ATCC (catalogue no. TIB-152) and cultured in RPMI 1640. RAW 264.7 cells were purchased from ATCC (catalogue no. TIB-71) and cultured in RPMI 1640. HeLa cells were a gift from P. Lehner (University of Cambridge) and were authenticated using short tandem repeat profiling (Eurofins Genomics). HeLa cells were cultured in DMEM. MEFs were isolated from macerated embryonic day (E) 12.5–13.5 embryos. A whole litter of embryos without sex selection were used. Stable transfection with SV40 large T antigen passage 3 was used for immortalization. Cells were subcultured over 17 more passages and maintained in DMEM⁶³. All media was supplemented with 10% FCS (catalogue no. 10270106, Gibco), 100 U ml⁻¹ penicillin and 100 µg ml⁻¹ streptomycin (catalogue no. P4333, Sigma-Aldrich). All cells were cultured in incubators with 5% CO₂ and at either 21% or 1% oxygen, as indicated. Low oxygen incubations were performed in

a Ruskin SCI-tive workstation. Cell number and viability was determined using the ADAM-MC Automated Cell Counter (NanoEntek), CellDrop Automated Cell Counter (DeNovix) or TC20 Automated Cell Counter (Bio-Rad Laboratories).

T cell isolation and activation

Human PBMCs were obtained from NHSBT: Addenbrooke's Hospital, Cambridge, UK or the Karolinska Hospital Service, Sweden. Ethical approval was obtained from the East of England-Cambridge Central Research Ethics Committee (06/Q0108/281) and consent was obtained from all participants. PBMCs from healthy donors were isolated from blood using discontinuous plasma Percoll gradients. Naive CD8⁺ T cells were isolated using the Naive CD8⁺ T Cell Isolation Kit (catalogue no. 130-093-244, Miltenyi Biotec), in accordance with the manufacturer's instructions. Total CD8⁺ T cells were purified by either positive or negative magnetic bead sorting (catalogue nos. 130-045-201 and 130-096-495, Miltenyi Biotec). All human CD8⁺ T cells were activated with anti-human CD3/CD28 Dynabeads (catalogue no. 11131D, Thermo Fisher Scientific) at a 1:1 cell:bead ratio and cultured in complete RPMI 1640 supplemented with 10% FCS, 100 U ml⁻¹ penicillin, 100 µg ml⁻¹ streptomycin and 30 U ml⁻¹ interleukin-2 (IL-2) (catalogue no. 11147528001, Sigma-Aldrich).

Mouse CD8⁺ T cells were isolated from mouse spleens using positive selection. Incubation with microbeads conjugated to monoclonal anti-mouse CD8α (Ly-2; isotype: rat IgG2a) antibody (catalogue no. 130-049-401, Miltenyi Biotec) was followed by magnetic bead isolation on a MACS column. WT mouse CD8⁺ T cells were activated with anti-mouse CD3/CD28 Dynabeads (catalogue no. 11453D, Thermo Fisher Scientific) at a 1:1 cell:bead ratio. Purified OT1 CD8⁺ T cells were activated with 1 µg ml⁻¹ of the OVA-derived peptide SIINFEKL (ProImmune). All mouse CD8⁺ T cells were cultured in complete RPMI 1640 supplemented with 10% FCS, 100 U ml⁻¹ penicillin, 100 µg ml⁻¹ streptomycin, 55 µM 2-ME (catalogue no. 21985023, Gibco) and 10 U ml⁻¹ IL-2.

Flow cytometry and sorting

Single-cell suspensions were stained with LIVE/DEAD Fixable Near-IR Dead Cell Stain Kit (catalogue no. 10119, Thermo Fisher Scientific) followed by surface and intracellular staining with fluorochrome-labelled antibodies (Supplementary Tables 1 and 2). Staining of cytoplasmic and nuclear antigens was performed using the Cytotfix/Cytoperm Fixation/Permeabilization Kit (catalogue no. 554714, BD Biosciences) and the Transcription Factor Buffer Set (catalogue no. 562725, BD Biosciences), respectively. For the proliferation assays, cells were loaded with CellTrace Violet (catalogue no. C34557, Thermo Fisher Scientific) according to the manufacturer's instructions. Samples were acquired on an Aurora (Cytek Biosciences).

For 5-hydroxymethylcytosine (5hmC) staining, cells were stained for surface antigens as above and then fixed and permeabilized with the Transcription Factor Buffer Set. Next cells were incubated with 4 M HCl for 10 min at room temperature. Cells were then thoroughly washed and incubated in blocking buffer (0.1% PBS-Triton X-100, 5% FCS) for 30 min at 4 °C. Cells were then incubated with primary anti-5hmC (catalogue no. 10013602, Active Motif) overnight at 4 °C and the day after with secondary antibody for 1 h at room temperature. Flow cytometry was then performed as explained above. Cells were sorted on an FACSAria III (BD Biosciences) after surface antigen staining as described above. Data were analysed using FlowJo v.10.7.2.

ELISA

Secreted IFN γ levels of cultured cells were determined using an ELISA. Assays were performed with uncoated ELISA kits (catalogue no. 88-7316, Thermo Fisher Scientific), according to the manufacturer's instructions. Absorbance was determined using a microplate reader (Sunrise, Tecan) at a wavelength of 450 nm.

Lentivirus transduction

To generate lentiviral particles, 5×10^6 HEK 293 cells were plated in 15-cm Petri dishes and transfected the day after with 50 μ l FuGENE (catalogue no. E2311, Promega Corporation), 10 μ g CAR-encoding vectors and 3.3 μ g of each third-generation lentivirus helper vectors (catalogue no. CART-027CL, Creative-Biolabs). Supernatant containing lentiviral particles was collected 48 h after transfection and used fresh or stored at -80°C . Lentiviral supernatant was spun onto non-treated plate wells coated with 30 $\mu\text{g ml}^{-1}$ RetroNectin reused up to three times (catalogue no. T100B, Takara Bio) at 2,000g for 2 h at 32°C and replaced with activated human CD8⁺ T cells in fresh RPMI 1640 supplemented with 30 U ml^{-1} IL-2.

In vitro cytotoxicity

Ten thousand B16F10-OVA or SKOV3 cells were seeded per well in 96-well plates and cocultured for a minimum of 14 h with varying ratios of mouse CD8⁺ OT1 or human CD8⁺ RQR8⁺ HER2 CAR T cells, respectively. T cells had been treated with or without DEG 7 days before the assay. Wells were washed twice with PBS to remove T cells and the number of remaining target cells was determined by culturing with 10 $\mu\text{g ml}^{-1}$ resazurin (catalogue no. R7017, Sigma-Aldrich) and measuring the fluorescence signal in a plate reader. Cytotoxicity was calculated relative to wells with no T cells added. Ten thousand Raji cells were cocultured for a minimum of 14 h with CD19 CAR T cells previously activated for 7 days and cultured with or without DEG. Cytotoxicity was assessed by flow cytometry using the ratio of live Raji cells to Count-Bright Absolute Counting Beads (catalogue no. C36950, Thermo Fisher Scientific). To determine specific cytotoxicity, data were normalized to the cytotoxicity of the vector-controlled transduced CD8 T cells of the respective donor.

Vectors

DNA encoding a codon-optimized polycistronic peptide consisting of RQR8 and anti-human HER2 (clone 4D5) interspersed with picornavirus T2A and furin cleavage sequences was synthesized by GeneScript. RQR8, used as the transduction marker, is a chimeric surface protein consisting of domains from CD34 (for detection and purification with clone QBEND/10), CD8 (for anchoring at the cell surface) and CD20 (for depletion in vivo with the anti-CD20 monoclonal antibody rituximab)⁶⁴. shRNA sequences corresponding to the best specificity score for each target were retrieved from the RNAi Consortium library. For coexpression of protein and shRNA, shRNA hairpins were flanked with an optimized sequence of miR-30 (refs. 65,66). 97-mer oligonucleotides (IDT Ultramers) coding for the respective shRNAs⁶⁷ were PCR-amplified using 10 μM of the primers miRE-XhoI-fw (5'-TGAACTCGAGAAGGTATATTGCTGTTGACAGTAGCG-3') and miRE-EcoRI-rev (5'-TCTCGAATTCTAGCCCCTTG AAGTCCGAGGCAGTAGGC-3'), a 0.5-ng oligonucleotide template and the Q5 High-Fidelity 2X Master Mix (New England Biolabs) and cloned into HER2 CAR vectors containing the miRE scaffold sequence. All coding sequences were cloned into pCDCAR1 (Creative Biolabs). Third-generation lentiviral transfer helper plasmids were obtained from Biocytogen. All sequences are available in Supplementary Table 3.^{65,67} The following lentiviral vectors purchased from Creative Biolabs were used: a truncated form of epidermal growth factor receptor (vector control) and anti-CD19 CAR with a 4-1BB endodomain.

Metabolite extraction and liquid chromatography–tandem mass spectrometry analysis

Metabolite extraction and liquid chromatography–tandem mass spectrometry analysis. Cells were counted to determine viable cell numbers (Fig. 1f,h,i and Extended Data Fig. g,h,k). A total of $0.5\text{--}2 \times 10^6$ viable cells were collected, washed with cold PBS and metabolic activity was quenched by freezing samples in dry ice and ethanol, and stored at -80°C . Metabolites were extracted by adding 150 μ l

ice-cold 1:1 (vol/vol) methanol/water (containing 1 mM *N*-cyclohexyl-2-aminoethanesulfonic acid (CHES) as an internal standard) to the cell pellets; samples were transferred to a chilled microcentrifuge tube containing 150 μ l chloroform and 500 μ l methanol (750 μ l total in 3:1:1 vol/vol methanol/water/chloroform). Samples were sonicated in a water bath for 8 min at 4°C , and centrifuged (13,000g) for 10 min at 4°C . The supernatant containing the extract was transferred to a new tube for evaporation using TurboVap LV (Biotage), resuspended in 3:3:1 (vol/vol/vol) methanol/water/chloroform (350 μ l total) to phase-separate polar metabolites from apolar metabolites and centrifuged. The aqueous phase was transferred to a new tube for evaporation using TurboVap LV, washed with 60 μ l methanol and dried again. Evaporated extracts were dissolved in 100 μ l MeOH–50% water, before injection on the machine. Isotopically labelled glutarates were determined by liquid chromatography (LC)–tandem mass spectrometry (tandem MS) on a Waters ACQUITY UPLC system coupled to a Xevo-TQ-XS mass spectrometer. A SeQuant ZIC-HILIC column (2.1 \times 100 mm, 3.5 μm , Merck) equipped with a guard column (ZIC-HILIC Guard, 20 \times 2.1 mm) was used for the separation, with mobile phase A consisting of MilliQ water, 0.1% v/v formic acid (FA) and mobile phase B consisting of acetonitrile, 0.1% v/v FA. The column was thermostated at 40°C , the injection volume was set to 3 μ l and the gradient was carried out at a flow rate of 0.3 ml min^{-1} as follows: 5% A from 0 to 1 min, linearly increased to 30% from minutes 1–5 and to 75% at minute 5.5. The column was subsequently washed in 75% A for 2.5 min and re-equilibrated at initial conditions for 3 min. MS analyses were performed in multiple reaction monitoring (MRM) mode, with positive electrospray ionization (ESI) from minute 0–1.4 and negative electrospray ionization (ESI) from minute 1.4 to minute 4.7. Positive ESI was conducted according to the following parameters: capillary potential 3 kV, source offset 30 V, cone voltage 15 V, source temperature 150°C , desolvation temperature 600°C , cone gas flow 150 l h^{-1} , desolvation gas flow, 1,000 l h^{-1} , nebulizer 7 bar and collision gas flow 0.17 ml min^{-1} . Negative ESI was operated under the same conditions but with a capillary potential set to 2 kV and a cone voltage set to 20 V. Acquisition was performed using MRM with the mass transitions and parameters illustrated in Supplementary Table 4. Two transitions were used for each of the target compounds and the ion ratio between them was used to increase the confidence in the identification. To account for instrumental variability, 1 mM CHES was spiked in the samples before cell lysis to be used as the volumetric internal standard.

Metabolite extraction and LC–MS analysis. Cells were counted to determine the viable cell numbers (Extended Data Fig. 1i,n). A total of $0.5\text{--}2 \times 10^6$ viable cells were collected, washed with cold PBS and metabolic activity was quenched by freezing samples in dry ice and ethanol and stored at -80°C . Before extraction, all samples were added with 10 μ l of the internal standard solution, consisting of 200 $\mu\text{g ml}^{-1}$ succinic acid-d4. Metabolites were subsequently extracted by adding 1,000 μ l ice-cold LC–MS-grade methanol to the cell pellets, followed by 30 min of sonication. Sonication was carried out by adding ice to the ultrasound bath to maintain the temperature below 20°C . After sonication, samples were centrifuged (12,000g, 20 min, 6°C) and 200 μ l of the supernatant were transferred to LC–MS vials for the subsequent analysis.

Glutarate was determined by LC–tandem MS on a Waters ACQUITY UPLC system coupled to a Xevo-TQ-S mass spectrometer (Waters). An ACQUITY Premier BEH Amide Vanguard Fit column (2.1 \times 100 mm, 1.7 μm), equipped with an integrated guard column, was used for the separation, with mobile phase A consisting of 20 mM ammonium formate + 0.1% FA in double deionized water and mobile phase B consisting of 0.1% FA in acetonitrile. The column was thermostated at 30°C , the injection volume was set to 2 μ l and the gradient was carried out at a flow rate of 0.35 ml min^{-1} as follows: 95% B from 0 to 1 min, linearly decreased to 55% B from minute 1 to minute 5 and to 45% B from minute

5 to minute 7, and increased back to 95% B in minutes 7–8.5. The column was subsequently re-equilibrated at initial conditions until minute 15.

MS analyses were performed using ESI with the following parameters: capillary potential –1.5 kV, source temperature 150 °C, desolvation temperature 550 °C, cone gas flow 150 l h⁻¹, desolvation gas flow 800 l h⁻¹, nebulizer 7 bar and collision gas flow 0.17 ml min⁻¹. Two selected reaction monitoring transitions were acquired for glutarate (131.0 > 69.2 and 131.0 > 113.1 as quantifier and qualifier transitions, respectively). The ion ratio between the transitions was used as an additional confirmation of the identification. For succinate-d₄, the 121.0 > 58.1 transition was used.

qPCR

Total RNA was extracted from isolated CD8⁺ T cells (RNeasy Kit, QIAGEN); 300 ng of RNA were used for complementary DNA synthesis (First-Strand cDNA Synthesis Kit, Invitrogen). Quantitative PCR with reverse transcription (RT–qPCR) was performed with SYBR green (Roche) in a StepOnePlus system (Applied Biosystems). All kits were used according to the manufacturer's instructions. Samples were run in technical duplicates. Primers were designed with NCBI primer blast and are listed in Supplementary Table 5.

Western blot

Cell pellets were lysed by either urea-Tris buffer (8 M urea, 50 mM Tris-HCl (pH 7.5), 150 mM β-mercaptoethanol), sonicated twice for 45 s intercalated with 1 min incubation on ice and centrifuged at 14,000g, 4 °C for 15 min or by RIPA Lysis and Extraction Buffer (catalogue no. 89900, Thermo Fisher Scientific), according to the manufacturer's instructions. Nuclear and cytosolic fractions were prepared from cells using the NE-PER kit (catalogue no. 78833, Thermo Fisher Scientific). Histones were extracted with the Histone Extraction Kit (catalogue no. ab113476, Abcam). Proteins were separated by SDS–PAGE and transferred to polyvinylidene fluoride (PVDF) membranes. Total protein stain was obtained using non-stain protein labelling reagent (catalogue no. A44448, Thermo Fisher Scientific). Membranes were then blocked in 5% milk prepared in PBS plus 0.05% Tween-20, incubated with primary antibodies overnight at 4 °C and horseradish peroxidase (HRP)-conjugated secondary antibodies (catalogue nos. HAF008 and HAF007, R&D Systems) for 1 h the next day. After enhanced chemiluminescence (ECL) exposure (catalogue no. GERPN2106, Sigma-Aldrich), membranes were imaged using an iBrightCL1000 (Thermo Fisher Scientific). The following primary antibodies from Cell Signaling Technology were used at a concentration of 1:1,000: anti-PDHK1 (catalogue no. 3820); anti-β-actin (catalogue no. 12262S); anti-PP1B (catalogue no. 43603); anti-OGDH (catalogue no. 26865S); anti-phospho-PDH α1 (catalogue no. 37115); anti-SIRT5 (catalogue no. 8779S); anti-H3 (catalogue no. 4499); anti-H3K4me2 (catalogue no. 9725); anti-H3K4me3 (catalogue no. 9751); anti-H3K9me2 (catalogue no. 4658); anti-H3K9me3 (catalogue no. 13969); anti-H3K27me2 (catalogue no. 9728); anti-H3K27me3 (catalogue no. 9733); anti-H3K36me2 (catalogue no. 2901); anti-H3K36me3 (catalogue no. 4909); anti-H3K79me2 (catalogue no. 5427); anti-H3K79me3 (catalogue no. 4360); anti-H3K9ac (catalogue no. 9649); anti-H3K18ac (catalogue no. 13998); and anti-H3K27ac (catalogue no. 8173). The following antibodies from Thermo Fisher Scientific were used at a concentration of 1:1,000: PDHc (catalogue no. 456799) and GCDH (catalogue no. PA5-60294). Other antibodies used at a concentration of 1:1,000 are as follows: pan anti-glutaryllysine (catalogue no. PTM-1151, PTM Biolabs) and anti-lipoic acid (catalogue no. 437695, Sigma-Aldrich).

For phosphorylation western blot analysis, stripping buffer (catalogue no. 21056, Thermo Fisher Scientific) was used for 15 min before membranes were re-blocked and stained for total protein as above.

Lipoic acid western blotting was performed as above with the following alterations: blocking buffer and secondary antibody buffer (5% milk plus 1% fatty acid free bovine serum albumin (BSA) (catalogue

no. BP9704100, Thermo Fisher Scientific) prepared in PBS plus 0.05% Tween-20); and primary antibody buffer (2% fatty acid free BSA prepared in PBS plus 0.05% Tween-20). Lipoic acid antibody was used at a concentration of 1:2,000 (catalogue no. 437695, Sigma-Aldrich). Data were analysed using the iBright Analysis Software v.4.0.1 or ImageJ.

In vitro TET2 and KDM4C enzymatic activity assay

A total of 2 nM of the human TET2 enzyme (catalogue no. 50162, BPS Bioscience) or 4 nM of the human KDM4C enzyme (catalogue no. 50105, BPS Bioscience) was incubated with the substrate of 30 nM single-stranded DNA (ssBiotin 26 nt Me-C Oligo, Genscript), in the presence of αKG (catalogue no. K3752, Sigma-Aldrich), 10 μM ammonium iron(II) sulphate hexahydrate (catalogue no. F3754, Sigma-Aldrich) in assay buffer (50 mM HEPES (catalogue no. 15630-080, Gibco), pH 7.0, 100 mM NaCl, 0.01% Pluronic F-127, 1 mM TCEP (S16054, Shanghai Yuanye Bio-Technology Company), 2 mM ascorbic acid (A5960, Sigma-Aldrich), 0.2 mg/ml BSA (catalogue no. B2064, Sigma-Aldrich) and 1,000 U ml⁻¹ catalase (catalogue no. C40, Sigma-Aldrich)). The concentration of αKG used for the TET2 standard and competitive assays was 115 μM and 4,500 μM, respectively. The concentration of αKG used for the KDM4C standard and competitive assays was 10 μM and 50 μM, respectively. The concentration of αKG used in the standard assay was calculated for each enzyme batch and is the concentration of substrate at which half the maximum reaction rate is achieved. DEG and glutaric acid were used in threefold serial dilution and the maximum concentration used was 5 mM. The pre-incubation time of the inhibitors with the TET2 mixture was 30 min at room temperature. The reaction step was at room temperature for 90 min. The product was detected by using a 5 nM anti-5hmC antibody (catalogue no. 39999, Active Motif), 5 nM Eu-Protein A (catalogue no. 61PRAKLB, Cisbio), 6.25 nM streptavidin-Alexa Fluor 647 (catalogue no. S21374, Thermo Fisher Scientific) and 10 mM EDTA (catalogue no. 0369, Sigma-Aldrich). For the standard curve, the ssBiotin 26 nt HydMe-C Oligo was used. The assays were performed in technical duplicates in a 384-well plate. Inhibitor analysis was performed within the linear range of catalysis.

The percentage of inhibition was calculated with the following formula: inhibition% = (1 – (signal value per well – average low control) / (average high control – average low control)) × 100. Data were fitted using Prism (GraphPad Software) with a four-parameter equation via 'log(inhibitor) versus response – variable slope' model.

In vitro HIF-P4H-1 and KDM6A activity assays

The human full-length HIF-P4H-1 and KDM6A enzymes were recombinantly produced using Sf21 insect cells and the enzymes were purified with anti-FLAG M2 affinity gel as described previously^{68,69}. Briefly, the C terminus FLAG-tagged human HIF-P4H1-2 and KDM6A were generated using PCR and subcloned into pAcG3X and pVL1393 baculovirus expression vectors, respectively. The recombinant baculoviruses were generated by transducing the bacmid DNA into *Spodoptera frugiperda* Sf9 cells using BaculoGold DNA (HIF-P4H1-2, BD Biosciences) and BacMagic-3 DNA kit (for KDM6A, Novagen). Recombinant proteins were produced by infecting Sf21 insect cells with the corresponding amplified baculoviruses for 72 h at 27 °C. Cells were homogenized in a buffer containing 10 mM Tris, 150 mM NaCl, 100 mM glycine, 0.1% (v/v) Triton X-100, pH 7.8, and a protease inhibitor cocktail tablet without EDTA. The cell lysates were centrifuged at 21,000g for 30 min; the soluble fractions containing the FLAG-tagged proteins were affinity-purified using the anti-FLAG M2 affinity gel (Sigma-Aldrich). The gel beads were washed with TBS buffer (50 mM Tris, 150 mM NaCl, pH 7.4, protease inhibitor cocktail tablet without EDTA) and the proteins were eluted with TBS buffer containing additionally 150 μg ml⁻¹ FLAG peptide. Protein concentration was measured with NanoDrop and proteins were analysed by SDS–PAGE followed by Coomassie brilliant blue staining. The inhibition assays were carried out using a method that measures the hydroxylation-coupled stoichiometric

release of $^{14}\text{CO}_2$ from 2-oxo-[1- ^{14}C] glutarate with a synthetic HIF-1 α peptide or a histone H3K27me3 peptide as substrates for HIF-P4H-1 and HIF-P4H-2 and KDM6A, respectively^{68,69}. Glutarate was used at increasing concentrations (50 μM to 10 mM) in the assay. The concentration of 2-oxoglutarate was 8 μM and 32 μM for the HIF-P4H-1 and KDM6A catalysed reactions, respectively, while keeping the concentrations of other cosubstrates and cofactors saturating and constant. The IC_{50} value of the glutarate analogue was calculated from the inhibition saturation curves.

HIF-PH cellular activity assays

MEFs were transiently transfected using Lipofectamine 2000 (Thermo Fisher Scientific) with 20 ng per expression plasmid for 2×10^4 cells per well in a 96-well plate. Cells were treated with transfection mixes for 8 h.

Generation of plasmids for the HIF-PH activity luciferase reporter assay has been described previously: luciferase reporter driven by GRE-luc pFLAG-Gal4-mHIF-1 α NTAD³⁵. Briefly, cells were concurrently transfected with pGRE-luc and a plasmid encoding constitutive expression of a fusion protein linking a FLAG-tagged Gal4 DNA-binding domain with one of the transcription activation domains of murine HIF-1 α . The NTAD contains proline residues that are hydroxylated by HIF-PH enzymes to target the protein for degradation; thus, luciferase expression is controlled by HIF-PH hydroxylation activity against the pFLAG-Gal4-mHIF-1 α NTAD. After 8 h of transient transfection with expression plasmids, cells were treated with experimental medium containing metabolites and drugs as described in the figure legends for 16 h; then, the luciferase signal assessed using the Steady-Glo Luciferase Assay System (Promega Corporation) detected using a luminometer. The luciferase signal was normalized to that induced by 2.5 mM DMOG.

IP of CD8⁺ T cells

A total of 30×10^6 CD8⁺ T cells were lysed with Pierce IP Lysis Buffer (catalogue no. 87787, Thermo Fisher Scientific). IP was performed using protein A Dynabeads (catalogue no. 10002D, Thermo Fisher Scientific) according to the manufacturer's instructions; 1–10 μg of target antibody was used per reaction. Eluted proteins were separated using SDS-PAGE, the gel was stained with InstantBlue Coomassie Protein Stain (catalogue no. ab119211, Abcam), imaged using an iBrightCL1000 and the stained target bands were cut and stored in water until analysis. Non-cut gels were transferred to PVDF membranes and then blocked in 5% milk prepared in PBS plus 0.05% Tween-20. Membranes were then incubated with primary antibodies overnight at 4 °C and HRP-conjugated secondary antibodies (HAF008 and HAF007) for 1 h the next day. After ECL exposure, membranes were imaged using an iBrightCL1000. The following primary antibodies were used at a concentration of 1:1,000; PDHc, OGDH and pan anti-glutaryllysine.

In-gel protein digestion and MS

Protein bands were excised manually from gels and in-gel digested using a MassPREP robotic protein-handling system (Waters). Gel pieces were destained according to the manufacturer's description. Then, proteins were reduced with 10 mM dithiothreitol (DTT) in 100 mM Ambic for 30 min at 40 °C and alkylated with 55 mM iodoacetamide in 100 mM Ambic for 20 min at 4 °C followed by digestion with 0.3 mg trypsin (sequence grade, Promega Corporation) in 50 mM Ambic for 5 h at 4 °C. The tryptic peptides were extracted with 1% FA in 2% acetonitrile, followed by 50% acetonitrile twice. The liquid was evaporated to dryness on a vacuum concentrator (Eppendorf).

The reconstituted peptides in solvent A (2% acetonitrile, 0.1% FA) were separated on a 50-cm long EASY-spray column (Thermo Fisher Scientific) connected to an UltiMate 3000 Nano-LC system (Thermo Fisher Scientific) using a 60-min gradient from 4% to 26% of solvent B (98% acetonitrile, 0.1% FA) in 55 min and up to 95% of solvent B in 5 min at a flow rate of 300 nL min⁻¹. Mass spectra were acquired on a Q Exactive HF Hybrid Orbitrap mass spectrometer (Thermo Fisher Scientific) in

m/z 375–1,500 at a resolution of $R = 120,000$ (at m/z 200) for full mass, followed by data-dependent higher-energy C-trap dissociation (HCD) fragmentations from 17 most intense precursor ions with a charge state 2+ to 7+. The tandem mass spectra were acquired with a resolution of $R = 30,000$, targeting 2×10^5 ions, setting the isolation width to m/z 1.4 and normalized collision energy to 28%.

Acquired raw data files were analysed using the Mascot Server v.2.5.1 (Matrix Science) and searched against the SwissProt protein database (20,368 human entries). A maximum of two missed cleavage sites were allowed for trypsin, while setting the precursor and the fragment ion mass tolerance to 10 ppm and 0.02 Da, respectively. Dynamic modifications of oxidation on methionine, deamidation of asparagine and glutamine, and acetylation of the *N* termini were set. Initial search results were filtered with a 5% false discovery rate using Percolator to recalculate Mascot scores. Protein identifications were accepted if they could be established at greater than 96.0% probability and contained at least two identified peptides. Proteins that contained similar peptides and could not be differentiated based on tandem MS analysis alone were grouped to satisfy the principles of parsimony.

IP and MS detection of lipoylation and glutarylation

HeLa cells were lysed on ice for 30 min in a HEPES buffer (150 mM NaCl, 50 mM HEPES, pH 7.0, 1% IGEPAL CA-630, 1 mM nicotinamide (Sigma-Aldrich), 5 mM Tris(2-carboxyethyl)phosphine hydrochloride (Sigma-Aldrich), 1 \times Complete Protease Inhibitor Cocktail (Roche) and 1 mM phenylmethylsulfonyl fluoride). Lysates were centrifuged at 14,000g for 10 min at 4 °C. Free thiols were blocked by adding 10 mM *N*-ethylmaleimide (NEM) (Sigma-Aldrich) and incubated on a rotator at 4 °C for 1 h. Lysates were immunoprecipitated by incubation with protein G Dynabeads (catalogue no. 10003D, Invitrogen), first for 1 h to pre-clear, and then overnight with the DLAT antibody (12362S (4A4-B6-C10), Cell Signaling Technology). Resins were washed four times with Tris-buffered saline containing 0.1% IGEPAL CA-630, followed by three washes with Tris-buffered saline. Protein was eluted using 2% SDS, 50 mM Tris, pH 7.4, 150 mM NaCl, 1 mM DTT and 10% glycerol, and incubated at 90 °C for 5 min. Proteins were then separated using NuPAGE 4–12% Bis-Tris gel (catalogue no. NP0321BOX, Invitrogen), and visualized using SimplyBlue SafeStain (Invitrogen).

Mass spectrometry data were acquired using an Orbitrap Fusion Lumos coupled to an UltiMate 3000 RSLCnano UHPLC equipped with a 100- μm ID \times 2 cm Acclaim PepMap Precolumn (Thermo Fisher Scientific) and a 75- μm ID \times 50 cm, 2- μm particle Acclaim PepMap RSLC analytical column. Loading solvent was 0.1% FA with analytical solvents A: 0.1% FA and B: 80% MeCN + 0.1% FA. Samples were loaded at 5 $\mu\text{L min}^{-1}$ loading solvent for 5 min before beginning the analytical gradient. The analytical gradient was 3–40% B over 42 min rising to 95% B by 45 min followed by a 4-min wash at 95% B and equilibration at 3% solvent B for 10 min. Columns were held at 40 °C. Data were acquired in a DDA fashion with the following settings: MS1: 380–1,500 Th, 120,000 resolution, 4×10^5 AGC target, 50-ms maximum injection time; MS2: quadrupole isolation at an isolation width of m/z 1.6, HCD fragmentation (NCE 30) with fragment ions scanning in the Orbitrap from m/z 110, 5×10^4 AGC target, 100-ms maximum injection time. Dynamic exclusion was set to ± 10 ppm for 60 s. MS2 fragmentation was triggered on precursors 5×10^4 counts and above.

Raw files were processed using PEAKS Studio (v.8.0, Bioinformatics Solutions) with the following parameters: enzyme: AspN, human database (UniProt reference proteome downloaded 21 January 2021 containing 20,541 proteins) with additional contaminant database (containing 246 common contaminants); variable modifications at PEAKS database stage: oxidation, carbamidomethylation, lipoylation, 1 \times and 2 \times NEM, glutaryl lipoate, NEM glutaryl lipoate and 309 built-in modifications at PEAKS PTM stage. The area under the curve (AUC) values for each peptide were extracted from the PEAKS peptide list, with AUCs calculated by PEAKS.

PDHc activity assay

PDHc activity was determined using a PDHc Activity Assay Kit (catalogue no. MAK183, Sigma-Aldrich). A total of 1×10^6 cells were used per reaction and the assay was performed according to the manufacturer's instructions. Activity was normalized to total protein concentration. Data were acquired on a FLUOstar Omega (BMG Labtech).

Seahorse

A Seahorse XFe bioanalyzer was used to measure the OCR and ECAR. A total of 1.5×10^5 CD8⁺ T cells per well were spun onto poly-D-lysine-coated (catalogue no. P7280, Sigma-Aldrich) Seahorse plates and preincubated at 37 °C for a minimum of 30 min in the absence of CO₂ in Seahorse XF RPMI medium, pH 7.4 (10376-100, Agilent), supplemented with 10 mM glucose (catalogue no. A2494001, Thermo Fisher Scientific) and 2 mM glutamine (catalogue no. 25030081, Thermo Fisher Scientific). A minimum of five technical replicates per biological replicate were used. For the MST and GST, OCR and ECAR were measured under basal conditions and after the addition of the following: 750 μM DEG (catalogue no. QB-1473, Combi-block), 0.05% DMSO, 1 μM oligomycin (catalogue no. 75351, Sigma-Aldrich), 1.5 μM FCCP (catalogue no. C2920, Sigma-Aldrich), 100 nM rotenone + 1 μM antimycin A (catalogue nos. R8875 and A8674, Sigma-Aldrich), 10 mM glucose and 50 mM 2-DG (catalogue no. B1048-100, BioVision) as indicated. To assess mitochondrial fuel use, OCR was measured subsequent to the addition of the following drugs in different combinations as indicated: 3 μM BPTES (catalogue no. SML0601, Sigma-Aldrich), 2 μM UK-5099 (catalogue no. PZ0160, Sigma-Aldrich) and 4 μM etomoxir (catalogue no. E1905, Sigma-Aldrich). Assay parameters were as follows: 3 min mix, no wait, 3 min measurement, repeated 3–5 times at basal and after each addition. Measurements were taken using a 96-well Extracellular Flux Analyzer (Seahorse Bioscience).

Glucose uptake assay

Glucose uptake was determined using a Glucose Uptake Assay Kit (catalogue no. J1341, Promega Corporation). The assay was performed according to the manufacturer's instructions. Data were acquired on the FLUOstar Omega.

Acetyl-CoA measurement

Acetyl-CoA levels were determined using an acetyl-CoA assay kit (catalogue no. MAK039, Sigma-Aldrich). After culture, 2×10^6 cells per condition were collected, washed twice with ice-cold PBS and resuspended in 500 μl of the assay buffer. Following deproteinization by adding 2 μl 1M perchloric acid, samples were sonicated and the assay was performed according to the manufacturer's instructions. Data were acquired on the FLUOstar Omega.

Orthotopic tumour growth and infiltration experiments

Eight to 15-week-old female NSG mice were inoculated subcutaneously with 1×10^6 SKOV3 and injected 21 days later with 5×10^5 RQR8⁺ human CD8⁺ CAR T cells expanded for seven days ex vivo. 100 U of IL-2 was injected peritoneally in NSG mice on the day of ACT and 3 days later. Animals were assigned randomly to each experimental group and tumour measurements were blinded. Tumour volume ($a \times b \times b/2$, where a is the length and b is the width) was measured every two to 3 days with electronic callipers until day 80. Tumour experiments using NSG mice were carried out with approval from the regional animal ethics committee of northern Stockholm, Sweden where the permitted maximal tumour volume of 1,000 cm³ was not exceeded.

Seven to 10-week-old male C57BL/6J mice were inoculated subcutaneously with 1.0×10^6 B16F10-OVA. Animals were assigned randomly to each experimental group. Four days after inoculation, mice were treated with a peritoneal injection of 0.2 mg DEG (approximately 10 mg kg⁻¹). Treatment was repeated every 2–3 days until day 28. Tumour volume was measured every 2–3 days with electronic

callipers until day 30. Peripheral blood was collected from the tail vein at day 7 and 14 days after tumour inoculation and analysed using flow cytometry. On day 14, tumours were dissected and dissociated using the Tumor Dissociation Kit (catalogue no. 130-095-929, Miltenyi Biotec), according to the manufacturer's instructions. Spleen and the tumour-draining lymph node were mashed in cell strainers. The tumour, spleen and draining lymph node single-cell suspensions were stained with fluorochrome-labelled antibodies and analysed using flow cytometry. The tumour experiments using C57BL/6J mice were carried out in accordance with the ethical regulations of the UK Home Office and the maximal tumour burden of 1,500 cm³ was not exceeded (mice were euthanized when tumour volume exceeded 1,000 cm³).

Statistics

Statistical analyses were performed with Prism 9 (GraphPad Software). $P < 0.05$ was considered statistically significant; the statistical tests used are stated in the figure legends.

Reporting summary

Further information on research design is available in the Nature Portfolio Reporting Summary linked to this article.

Data availability

All data generated or analysed during this study are included in the published article and its supplementary information files. The data that support the findings of this study are available from the corresponding author upon reasonable request. Source data are provided with this paper.

Code availability

No code was used in this study.

References

1. Kaech, S. M. & Cui, W. Transcriptional control of effector and memory CD8⁺ T cell differentiation. *Nat. Rev. Immunol.* **12**, 749–761 (2012).
2. Sallusto, F., Lanzavecchia, A., Araki, K. & Ahmed, R. From vaccines to memory and back. *Immunity* **33**, 451–463 (2010).
3. Crompton, J. G. et al. Lineage relationship of CD8⁺ T cell subsets is revealed by progressive changes in the epigenetic landscape. *Cell Mol. Immunol.* **13**, 502–513 (2016).
4. Harland, K. L. et al. Epigenetic plasticity of Cd8a locus during CD8⁺ T-cell development and effector differentiation and reprogramming. *Nat. Commun.* **5**, 3547 (2014).
5. Russ, B. E. et al. Distinct epigenetic signatures delineate transcriptional programs during virus-specific CD8⁺ T Cell differentiation. *Immunity* **41**, 853–865 (2014).
6. Wei, J., Raynor, J., Nguyen, T.-L. M. & Chi, H. Nutrient and metabolic sensing in T cell responses. *Front. Immunol.* **8**, 247 (2017).
7. Kedia-Mehta, N. & Finlay, D. K. Competition for nutrients and its role in controlling immune responses. *Nat. Commun.* **10**, 2123 (2019).
8. Palazon, A. et al. An HIF-1α/VEGF-A axis in cytotoxic T cells regulates tumor progression. *Cancer Cell* **32**, 669–683 (2017).
9. Ross, S. H., Rollings, C. M. & Cantrell, D. A. Quantitative analyses reveal how hypoxia reconfigures the proteome of primary cytotoxic T lymphocytes. *Front. Immunol.* **12**, 712402 (2021).
10. Caldwell, C. C. et al. Differential effects of physiologically relevant hypoxic conditions on T lymphocyte development and effector functions. *J. Immunol.* **167**, 6140–6149 (2001).
11. Tyrakis, P. A. et al. S-2-hydroxyglutarate regulates CD8⁺ T-lymphocyte fate. *Nature* **540**, 236–241 (2016).
12. Foskolou, I. P. et al. The S enantiomer of 2-hydroxyglutarate increases central memory CD8 populations and improves CAR-T therapy outcome. *Blood Adv.* **4**, 4483–4493 (2020).

13. Bunse, L. et al. Suppression of antitumor T cell immunity by the oncometabolite (R)-2-hydroxyglutarate. *Nat. Med.* **24**, 1192–1203 (2018).
14. Laukka, T. et al. Fumarate and succinate regulate expression of hypoxia-inducible genes via TET enzymes. *J. Biol. Chem.* **291**, 4256–4265 (2016).
15. Koivunen, P. et al. Inhibition of hypoxia-inducible factor (HIF) hydroxylases by citric acid cycle intermediates: possible links between cell metabolism and stabilization of HIF. *J. Biol. Chem.* **282**, 4524–4532 (2007).
16. Koivunen, P. et al. Transformation by the (R)-enantiomer of 2-hydroxyglutarate linked to EGLN activation. *Nature* **483**, 484–488 (2012).
17. Chowdhury, R. et al. The oncometabolite 2-hydroxyglutarate inhibits histone lysine demethylases. *EMBO Rep.* **12**, 463–469 (2011).
18. Xiao, M. et al. Inhibition of α -KG-dependent histone and DNA demethylases by fumarate and succinate that are accumulated in mutations of FH and SDH tumor suppressors. *Gene Dev.* **26**, 1326–1338 (2012).
19. Baksh, S. C. & Finley, L. W. S. Metabolic coordination of cell fate by α -ketoglutarate-dependent dioxygenases. *Trends Cell Biol.* **31**, 24–36 (2020).
20. Losman, J.-A., Koivunen, P. & Kaelin, W. G. Jr 2-Oxoglutarate-dependent dioxygenases in cancer. *Nat. Rev. Cancer* **20**, 710–726 (2020).
21. Morris, J. P. 4th et al. Ketoglutarate links p53 to cell fate during tumour suppression. *Nature* **573**, 595–599 (2019).
22. Gholson, R. K., Sanders, D. C. & Henderson, L. M. Glutaric acid: a product of tryptophan metabolism. *Biochem. Biophys. Res. Commun.* **1**, 98–100 (1959).
23. Borsook, H., Deasy, C. L., Haagen-Smit, A. J., Keighley, G. & Lowy, P. H. The degradation of α -amino adipic acid in guinea pig liver homogenate. *J. Biol. Chem.* **176**, 1395–1400 (1948).
24. Dwyer, T. M., Rao, K. S., Goodman, S. I. & Frerman, F. E. Proton abstraction reaction, steady-state kinetics, and oxidation–reduction potential of human glutaryl-CoA dehydrogenase. *Biochemistry* **39**, 11488–11499 (2000).
25. Marlaire, S., Schaftingen, E. V. & Veiga-da-Cunha, M. C7orf10 encodes succinate-hydroxymethylglutarate CoA-transferase, the enzyme that converts glutarate to glutaryl-CoA. *J. Inherit. Metab. Dis.* **37**, 13–19 (2013).
26. Goodman, S. I., Markey, S. P., Moe, P. G., Miles, B. S. & Teng, C. C. Glutaric aciduria; A “new” disorder of amino acid metabolism. *Biochem. Med.* **12**, 12–21 (1975).
27. Strauss, K. A., Puffenberger, E. G., Robinson, D. L. & Morton, D. H. Type I glutaric aciduria, part 1: natural history of 77 patients. *Am. J. Med. Genet. C Semin. Med. Genet.* **121C**, 38–52 (2003).
28. Kyllerman, M. et al. Long-term follow-up, neurological outcome and survival rate in 28 Nordic patients with glutaric aciduria type 1. *Eur. J. Paediatr. Neurol.* **8**, 121–129 (2004).
29. Kölker, S., Ahlemeyer, B., Krieglstein, J. & Hoffmann, G. F. Evaluation of trigger factors of acute encephalopathy in glutaric aciduria type I: fever and tumour necrosis factor- α . *J. Inherit. Metab. Dis.* **23**, 359–362 (2000).
30. Howden, A. J. M. et al. Quantitative analysis of T cell proteomes and environmental sensors during T cell differentiation. *Nat. Immunol.* **20**, 1542–1554 (2019).
31. Lukashev, D., Caldwell, C., Ohta, A., Chen, P. & Sitkovsky, M. Differential regulation of two alternatively spliced isoforms of hypoxia-inducible factor-1 α in activated T lymphocytes. *J. Biol. Chem.* **276**, 48754–48763 (2001).
32. Veliça, P. et al. Modified hypoxia-inducible factor expression in CD8⁺ T cells increases antitumor efficacy. *Cancer Immunol. Res.* **9**, 401–414 (2021).
33. Sekine, T. et al. TOX is expressed by exhausted and polyfunctional human effector memory CD8⁺ T cells. *Sci. Immunol.* **5**, eaba7918 (2020).
34. Khan, O. et al. TOX transcriptionally and epigenetically programs CD8⁺ T cell exhaustion. *Nature* **571**, 211–218 (2019).
35. Pereira, T., Zheng, X., Ruas, J. L., Tanimoto, K. & Poellinger, L. Identification of residues critical for regulation of protein stability and the transactivation function of the hypoxia-inducible factor-1 α by the von Hippel–Lindau tumor suppressor gene product. *J. Biol. Chem.* **278**, 6816–6823 (2003).
36. Tan, M. et al. Lysine glutarylation is a protein posttranslational modification regulated by SIRT5. *Cell Metab.* **19**, 605–617 (2014).
37. Bao, X. et al. Glutarylation of histone H4 lysine 91 regulates chromatin dynamics. *Mol. Cell* **76**, 660–675 (2019).
38. Xie, L. et al. Functions and mechanisms of lysine glutarylation in eukaryotes. *Front. Cell Dev. Biol.* **9**, 667684 (2021).
39. Schmiesing, J. et al. Disease-linked glutarylation impairs function and interactions of mitochondrial proteins and contributes to mitochondrial heterogeneity. *Cell Rep.* **24**, 2946–2956 (2018).
40. Patel, M. S., Nemeria, N. S., Furey, W. & Jordan, F. The pyruvate dehydrogenase complexes: structure-based function and regulation. *J. Biol. Chem.* **289**, 16615–16623 (2014).
41. Green, J. D., Perham, R. N., Ullrich, S. J. & Appella, E. Conformational studies of the interdomain linker peptides in the dihydrolipoyl acetyltransferase component of the pyruvate dehydrogenase multienzyme complex of *Escherichia coli*. *J. Biol. Chem.* **267**, 23484–23488 (1992).
42. Bleile, D. M., Munk, P., Oliver, R. M. & Reed, L. J. Subunit structure of dihydrolipoyl transacetylase component of pyruvate dehydrogenase complex from *Escherichia coli*. *Proc. Natl Acad. Sci. USA* **76**, 4385–4389 (1979).
43. Stephens, P. E., Darlison, M. G., Lewis, H. M. & Guest, J. R. The pyruvate dehydrogenase complex of *Escherichia coli* K12. Nucleotide sequence encoding the pyruvate dehydrogenase component. *Eur. J. Biochem.* **133**, 155–162 (1983).
44. Perham, R. N., Duckworth, H. W. & Roberts, G. C. Mobility of polypeptide chain in the pyruvate dehydrogenase complex revealed by proton NMR. *Nature* **292**, 474–477 (1981).
45. Packman, L. C., Green, B. & Perham, R. N. Lipoylation of the E2 components of the 2-oxo acid dehydrogenase multienzyme complexes of *Escherichia coli*. *Biochem. J.* **277**, 153–158 (1991).
46. Bevilacqua, A., Li, Z. & Ho, P.-C. Metabolic dynamics instruct CD8⁺ T-cell differentiation and functions. *Eur. J. Immunol.* **52**, 541–549 (2022).
47. Elia, I. et al. Tumor cells dictate anti-tumor immune responses by altering pyruvate utilization and succinate signaling in CD8⁺ T cells. *Cell Metab.* **34**, 1137–1150 (2022).
48. Pardee, T. S. et al. A phase I study of CPI-613 in combination with high dose cytarabine and mitoxantrone for relapsed or refractory acute myeloid leukemia. *Clin. Cancer Res.* **24**, 2060–2073 (2018).
49. Philip, P. A. et al. A phase III open-label trial to evaluate efficacy and safety of CPI-613 plus modified FOLFIRINOX (mFFX) versus FOLFIRINOX (FFX) in patients with metastatic adenocarcinoma of the pancreas. *Future Oncol.* **15**, 3189–3196 (2019).
50. Dionisio, K. L. et al. The Chemical and Products Database, a resource for exposure-relevant data on chemicals in consumer products. *Sci. Data* **5**, 180125 (2018).
51. Russi, A. S. et al. Malignant brain tumors in patients with glutaric aciduria type I. *Mol. Genet. Metab.* **125**, 276–280 (2018).
52. Carty, S. A. et al. The loss of TET2 promotes CD8⁺ T cell memory differentiation. *J. Immunol.* **200**, 82–91 (2018).
53. Fraietta, J. A. et al. Disruption of TET2 promotes the therapeutic efficacy of CD19-targeted T cells. *Nature* **558**, 307–312 (2018).

54. Scharer, C. D., Bally, A. P. R., Gandham, B. & Boss, J. M. Cutting edge: chromatin accessibility programs CD8 T cell memory. *J. Immunol.* **198**, 2238–2243 (2017).
55. Verma, S. NRF2 mediates melanoma addiction to GCDH by modulating apoptotic signalling. *Nat. Cell Biol.* **24**, 1422–1432 (2022).
56. Bhatt, D. P. et al. Deglutarylation of glutaryl-CoA dehydrogenase by deacylating enzyme SIRT5 promotes lysine oxidation in mice. *J. Biol. Chem.* **298**, 101723 (2022).
57. Cheng, Y.-M. et al. Lysine glutarylation in human sperm is associated with progressive motility. *Hum. Reprod.* **34**, 1186–1194 (2019).
58. Zhou, L. et al. SIRT5 promotes IDH2 desuccinylation and G6PD deglutarylation to enhance cellular antioxidant defense. *EMBO Rep.* **17**, 811–822 (2016).
59. Bailey, P. S. J. et al. ABHD11 maintains 2-oxoglutarate metabolism by preserving functional lipoylation of the 2-oxoglutarate dehydrogenase complex. *Nat. Commun.* **11**, 4046 (2020).
60. Seim, G. L. et al. Nitric oxide-driven modifications of lipoic arm inhibit α -ketoacid dehydrogenases. *Nat. Chem. Biol.* **19**, 265–274 (2023).
61. Mathias, R. A. et al. Sirtuin 4 is a lipoamidase regulating pyruvate dehydrogenase complex activity. *Cell* **159**, 1615–1625 (2014).
62. Ryan, H. E., Lo, J. & Johnson, R. S. HIF-1 α is required for solid tumor formation and embryonic vascularization. *EMBO J.* **17**, 3005–3015 (1998).
63. Sim, J. et al. The factor inhibiting HIF asparaginyl hydroxylase regulates oxidative metabolism and accelerates metabolic adaptation to hypoxia. *Cell Metab.* **27**, 898–913 (2018).
64. Philip, B. et al. A highly compact epitope-based marker/suicide gene for easier and safer T-cell therapy. *Blood* **124**, 1277–1287 (2014).
65. Bofill-De Ros, X. & Gu, S. Guidelines for the optimal design of miRNA-based shRNAs. *Methods* **103**, 157–166 (2016).
66. Fellmann, C. et al. An optimized microRNA backbone for effective single-copy RNAi. *Cell Rep.* **5**, 1704–1713 (2013).
67. Moffat, J. et al. A lentiviral RNAi library for human and mouse genes applied to an arrayed viral high-content screen. *Cell* **124**, 1283–1298 (2006).
68. Hirsilä, M., Koivunen, P., Günzler, V., Kivirikko, K. I. & Myllyharju, J. Characterization of the human prolyl 4-hydroxylases that modify the hypoxia-inducible factor. *J. Biol. Chem.* **278**, 30772–30780 (2003).
69. Chakraborty, A. A. et al. Histone demethylase KDM6A directly senses oxygen to control chromatin and cell fate. *Science* **363**, 1217–1222 (2019).

Acknowledgements

We thank A. Vegvari and the Karolinska Institute Small Molecule Mass Spectrometry Core Facility, supported by KI/SL for support in sample analysis and scientific input. In-gel digestion, peptide extraction, mass spectrometry analysis and database searches for protein identification were carried out with thanks at the Proteomics Biomedicum, Karolinska Institute, Stockholm (<https://ki.se/en/mbb/proteomics-biomedicum>). We thank P. Tyrakis for work at the initiation of this effort, and P. Hamblin and D. Cawkill of Apollo Therapeutics for helpful suggestions and advice. We thank C. M. Branco of Queen's University, Belfast for helpful discussions and unpublished experimental work, and the recruitment and support of P.P. Cunha. We thank the animal staff at the Gurdon Institute Cambridge and Karolinska Institute for animal and technical assistance. We thank the flow cytometry facility at the School of the Biological Sciences, Cambridge for their support and assistance in this work. We thank

N. E. Sajgo for assistance with schematic generation. This work was funded by a Wellcome Trust Principal Research Fellowship award (214283/Z/19/Z), a Knut and Alice Wallenbergs Stiftelse Scholar award, a Vetenskapsrådet award (2019-01485), a Cancerfonden award (CAN2018/808) and a Barncancerfonden award (PR2020-007) to R.S.J.; the Evelyn Trust Cambridge (Patrick Sisson's Research Fellowship) and the Karolinska Institute Jonas Söderquists Fellowship awarded to I.P.F.; the Portuguese Foundation for Science and Technology scholarship (SFRH/BD/115612/2016) awarded to P.P.C.; a Canadian Institutes of Health Research Fellowship (MFE176599) to B.J.W.; a Wellcome Senior Fellowship to J.A.N. (215477/Z/19/Z); and a Lister Institute of Preventive Medicine Fellowship to J.A.N.

Author contributions

E.M., P.P.C., J.A.N., I.P.F. and R.S.J. conceptualized the study. E.M. and P.P.C. devised the methodology. E.M. carried out the formal analysis. E.M., P.P.C., B.J.W., G.L.G., S.K.S.-T., R.H., A.Q., J.Z., R.A. and L.B. carried out the investigation. E.M. wrote the original manuscript draft. E.M., P.P.C., P.V., D.B., C.E.W., P.K., I.P.F., J.A.N. and R.S.J. reviewed and edited the manuscript. R.S.J. managed the project. R.S.J. acquired the primary funding.

Competing interests

The authors declare no competing interests.

Additional information

Extended data is available for this paper at <https://doi.org/10.1038/s42255-023-00855-2>.

Supplementary information The online version contains supplementary material available at <https://doi.org/10.1038/s42255-023-00855-2>.

Correspondence and requests for materials should be addressed to Randall S. Johnson.

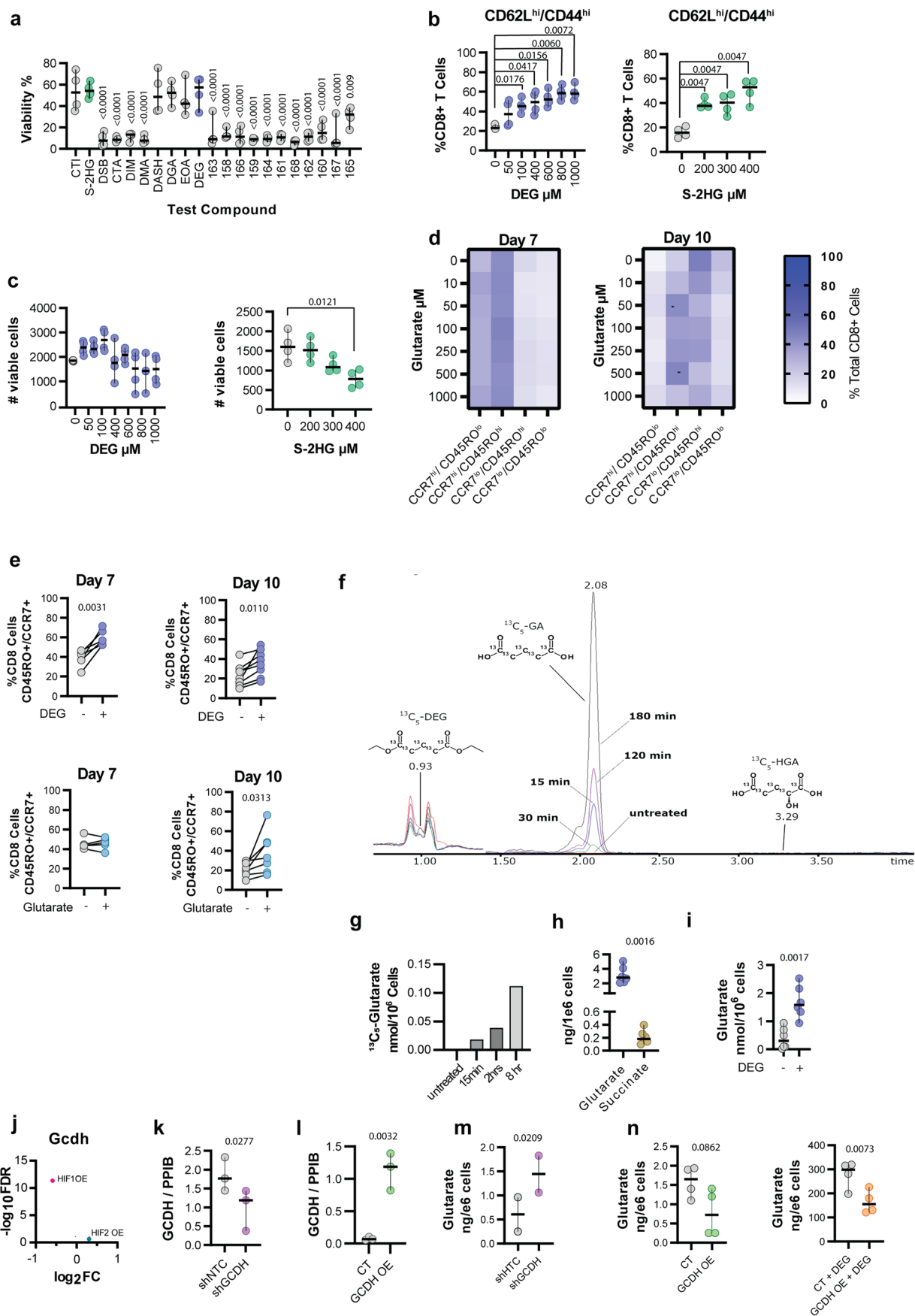
Peer review information *Nature Metabolism* thanks Matthew Hirschev and the other, anonymous, reviewer(s) for their contribution to the peer review of this work. Primary Handling Editor: Alfredo Giménez-Cassina, in collaboration with the *Nature Metabolism* team.

Reprints and permissions information is available at www.nature.com/reprints.

Publisher's note Springer Nature remains neutral with regard to jurisdictional claims in published maps and institutional affiliations.

Open Access This article is licensed under a Creative Commons Attribution 4.0 International License, which permits use, sharing, adaptation, distribution and reproduction in any medium or format, as long as you give appropriate credit to the original author(s) and the source, provide a link to the Creative Commons license, and indicate if changes were made. The images or other third party material in this article are included in the article's Creative Commons license, unless indicated otherwise in a credit line to the material. If material is not included in the article's Creative Commons license and your intended use is not permitted by statutory regulation or exceeds the permitted use, you will need to obtain permission directly from the copyright holder. To view a copy of this license, visit <http://creativecommons.org/licenses/by/4.0/>.

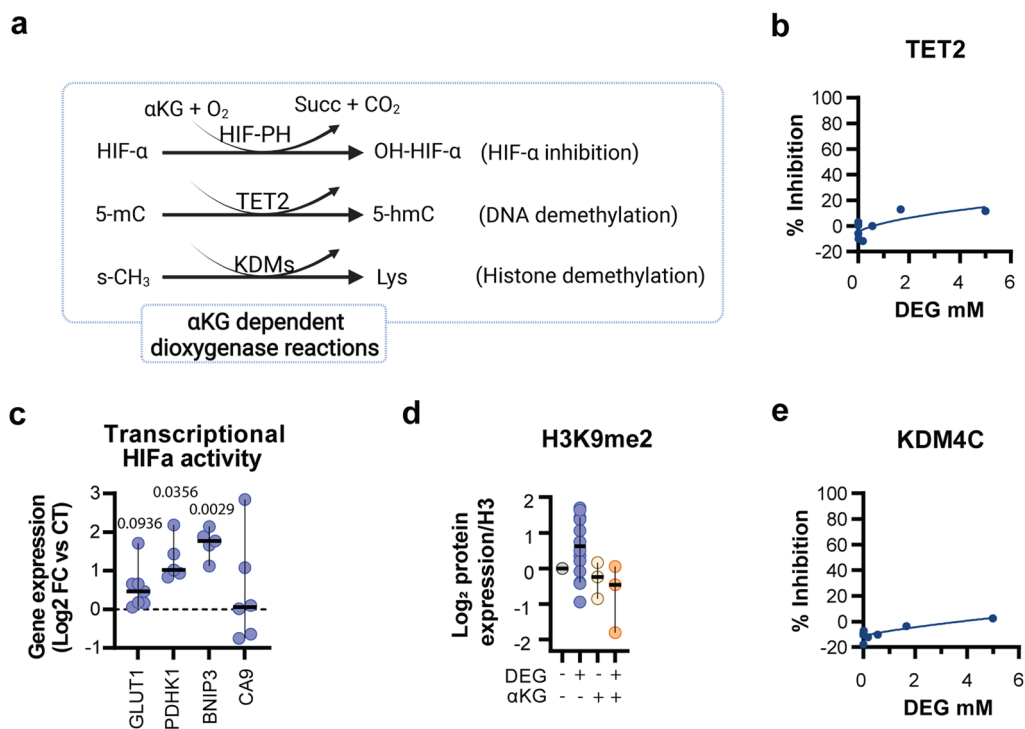
© The Author(s) 2023



Extended Data Fig. 1 | See next page for caption.

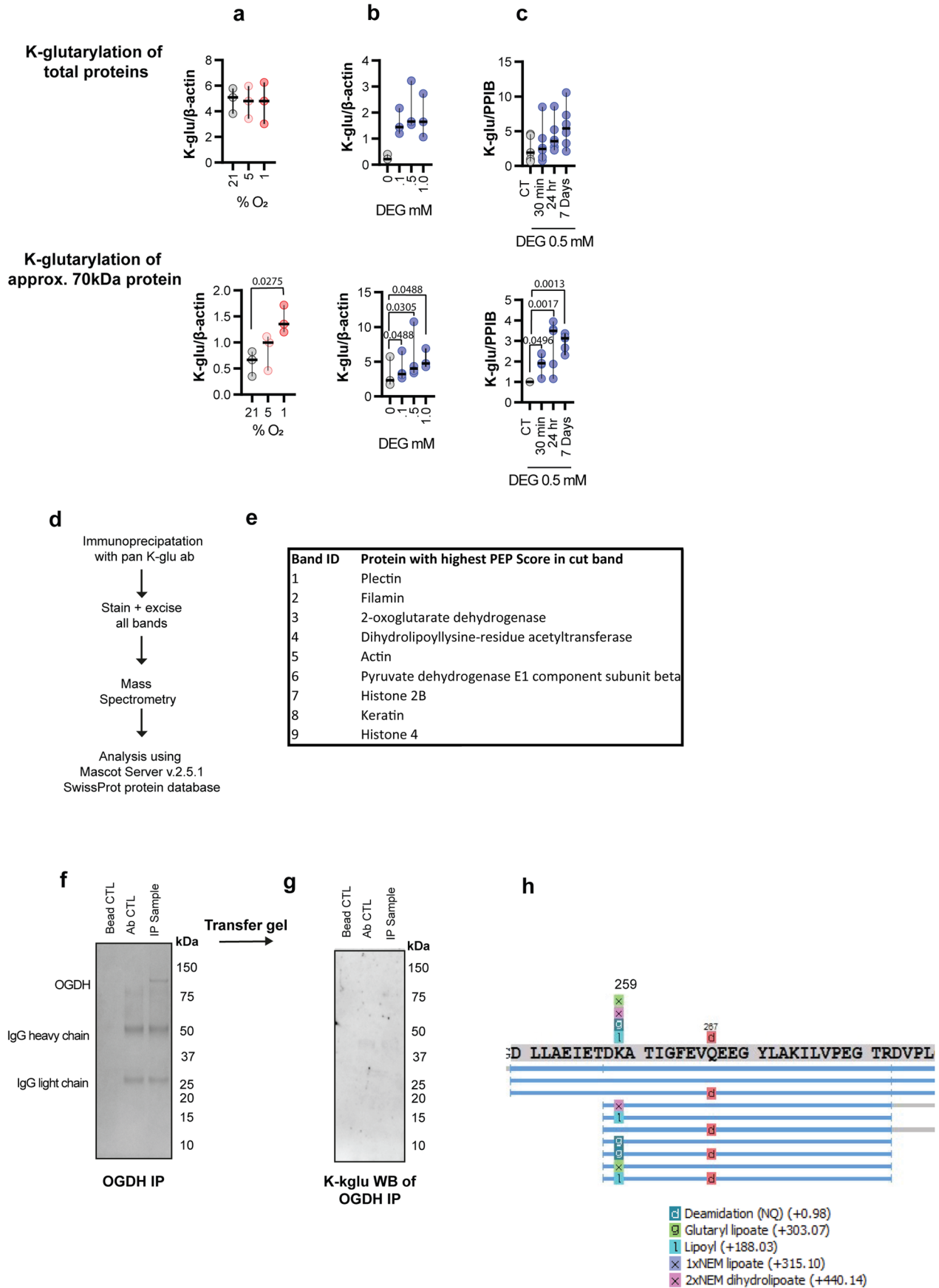
Extended Data Fig. 1 | Glutarate is an endogenous regulator of CD8⁺ T cell function. **a**, Percentage viability of murine CD8⁺ T cells following 7 days of treatment with 400 μ M of test compound, as determined by flow cytometry. Ordinary one-way ANOVA relative to CT; n = 4. **b**, Percentage of murine CD62L^{hi}/CD44^{hi} CD8⁺ T cells following 7 days of treatment with increasing concentrations of DEG (left) or S-2HG (right). Ordinary one-way ANOVA; n = 4. **c**, Number of viable murine CD8⁺ cells following 7 days of treatment with increasing concentration of DEG (right) or S-2HG (left), as determined by counting beads and flow cytometry. Ordinary one-way ANOVA relative to CT; n = 4. **d**, Heatmap representing the proportion of human CD8⁺ T cells expressing CCR7/CD45RO following 7 or 10 days treatment with increasing concentrations of DEG. Two-way ANOVA relative to CT; n = 4-5. **e**, Percentage of CD62L^{hi}/CD44^{hi} human CD8⁺ T cells human 7- or 10-days culture with DEG 500 μ M or Glutarate 500 μ M. Two-tailed paired t-test; DEG 7 days n = 6; DEG 10 days n = 8, Glutarate 7 days n = 5; Glutarate 10 days n = 8. **f**, Chromatograms of isotope tracing. Human CD8⁺ T cells were treated with ¹³C₅-DEG for varying time length and mass

spectrometry for glutarate was performed. **g**, Quantified ¹³C₅-Glutarate from cells treated as described and shown as chromatograms in Extended Data Fig. 1f. **h**, Glutarate and succinate levels in activated human CD8⁺ T cells. Two-tailed paired t-test; n = 6. **i**, Glutarate levels in CD8⁺ T cells cultured +/- DEG 500 μ M for 7 days. Two-tailed paired t-test; n = 6. **j**, *Gcdh* levels in transcripts HIF1 OE (HIF1AAA) and HIF2 OE (HIF2AAA) – transduced mouse CD8⁺ T cells, relative to vector control³⁴. **k**, GCDH levels in T cells transduced with an shNTC or shGCDH vectors as determined by western blot analysis. Two-tailed paired t-test; n = 3. **l**, GCDH levels in T cells transduced with a CT or GCDH overexpressing vector as determined by western blot analysis. Two-tailed paired t-test; n = 3. **m**, Glutarate levels in HEK293 cells transduced with shGCDH overexpressing vectors used in Fig. 1k and Extended Data Fig. 1k. Two-tailed paired t-test; n = 2. **n**, Glutarate levels in HEK293 cells transduced with GCDH overexpressing vectors and treated with 500 μ M and used in Fig. 1k and Extended Data Fig. 1l. Two-tailed paired t-test; n = 4. All scatter plots and bar charts show median and 95% CI where each dot represents one human donor. *p < 0.05.



Extended Data Fig. 2 | Glutarate is an inhibitor of αKGDDs. **a**, Illustration of alpha-ketoglutarate (αKG) dependent dioxygenase (αKGDD) reactions investigated in this study. (*Adapted from BioRender.com*) **b**, Cell free enzymatic inhibition assay for TET2 using increasing concentrations of DEG. **c**, qPCR analysis of CD8⁺ T cells treated with 500 μM DEG for 7 days. Each dot represents one human donor relative to untreated donor control (dotted black line), normalised to HPRT. Two-tailed one sample t-test; GLUT1 n = 8; PDHK1 n = 5;

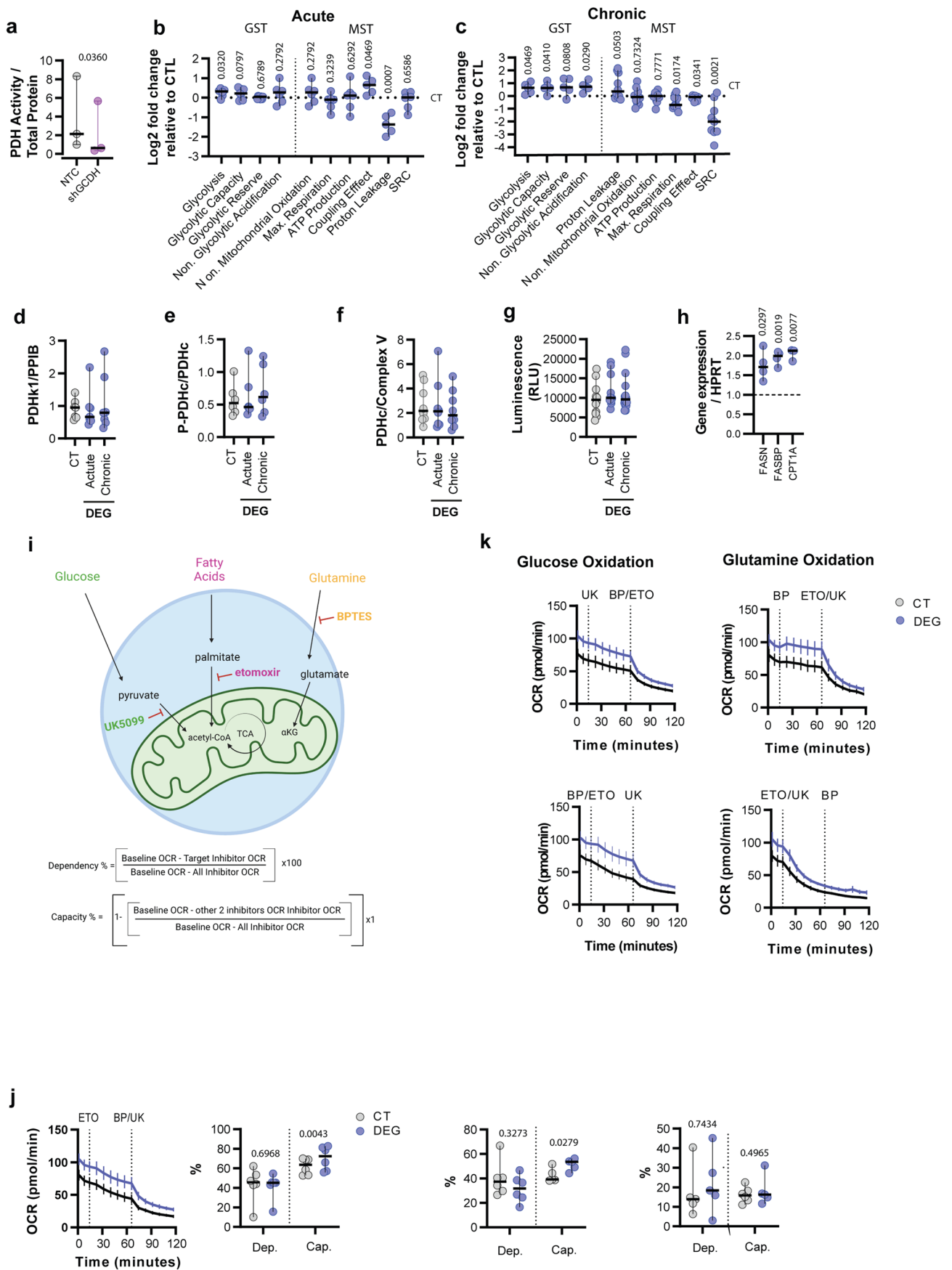
BNIP3 n = 5; CA9 n = 6. **d**, Log₂ FC protein expression of H3K9me2 in human CD8⁺ T cells treated with +/- 500 μM DEG and 500 μM αKG for 7 days. Ordinary one-way ANOVA; DEG n = 11, αKG n = 3; αKG + DEG n = 3. **e**, Cell free enzymatic inhibition assay for TET2 using increasing concentrations of glutarate and 5x αKG than in Fig. 2i. Cell free enzymatic assay graphs show Michaelis-Menten line of best fit of at least 3 independent experiments. All scatter plots show median + 95% CI, where each dot represents one donor as indicated.



Extended Data Fig. 3 | See next page for caption.

Extended Data Fig. 3 | Glutarylation of pyruvate dehydrogenase disrupts lipoylation. **a**, Quantified total protein lysine-glutarylation or lysine-glutarylation of 67-70 kDa protein, as determined by western blot analysis and relative to β -actin, of human CD8⁺ T cells which were cultured at different oxygen tensions for 24 h prior to harvest (as in described in Fig. 4c). Ordinary one-way ANOVA; n = 3. **b**, Quantified total protein lysine-glutarylation or lysine-glutarylation of 67-70 kDa protein, as determined by western blot analysis and relative to β -actin, of cells treated with increasing concentrations of DEG for 7 days (as described in Fig. 4d). Ordinary one-way ANOVA; n = 3. **c**, Quantified total protein lysine-glutarylation or lysine-glutarylation of 67-70 kDa protein, as determined by western blot analysis and relative to PPIB, of human CD8⁺ T cells 7 days post activation. Cells were treated with DEG 500 μ M for different time lengths as indication and harvested at the same time 7 days post activation (as described in Fig. 4e). Ordinary one-way ANOVA; n = 5. **d**, Model of

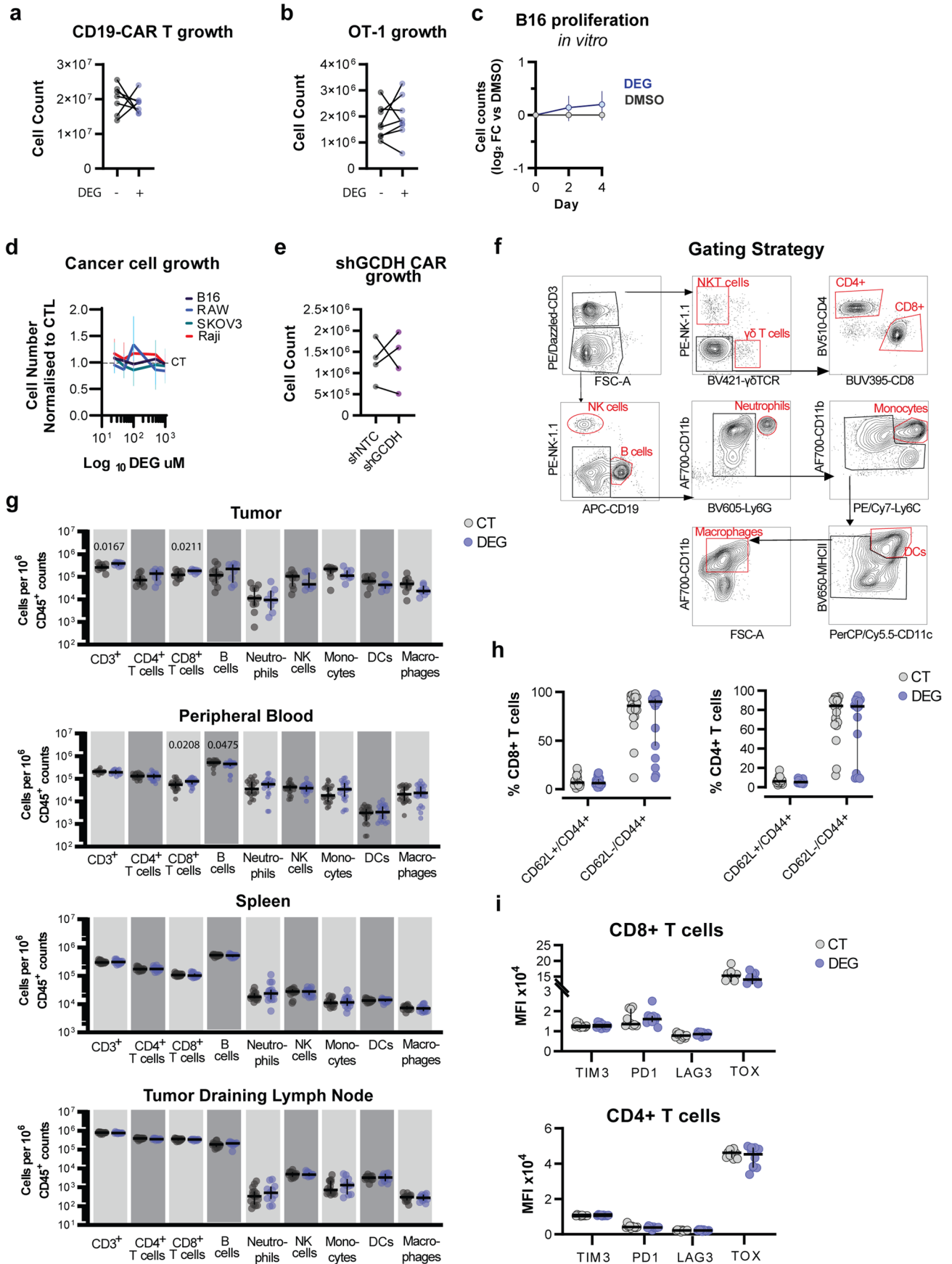
lysine-glutarylated protein isolation and identification by mass spectrometry. Lysine-glutarylation immunoprecipitation was performed on 30×10^6 mouse CD8⁺ T cells, 7 days post activation. Following protein separation by SDS-PAGE, gel was stained with Coomassie blue and stained bands were excised, gel was digested and mass spectrometry was performed. Data was analysed using the Mascot Server v.2.3.1 and the SwissProt protein database. 3 independent experiments and analysis performed. **e**, Top hits for each excised band from mass spectrometry described in Fig. 4g. **f**, Representative immunoprecipitation of Oxoglutarate dehydrogenase (OGDH) complex isolated from 30×10^6 mouse CD8⁺ T cells by immunoprecipitation. N = 3. **g**, Representative K-glutarylation western blot of immunoprecipitated OGDH complex as described in Extended Data Fig. 4f. N = 3. **h**, Schematic illustrating PEAKS PTM K259 on PDHE2 (selected modifications). All scatter plots show median and 95% CI where each dot represents one human donor.



Extended Data Fig. 4 | See next page for caption.

Extended Data Fig. 4 | Glutarate modulates mitochondrial function by inhibiting pyruvate dehydrogenase. **a**, PDHc activity of CD8⁺ T cells transduced with a NTC or shGCDH normalised to total protein. Two-tailed unpaired t-test; n = 3. **b-c**, Quantitative analysis of MST and GST following acute (30 min) (left) and chronic (7 days) (right) DEG exposure, as described in Fig. 4c-d and Fig. 4h-i, shown as log₂ FC relative to untreated control (black dotted line). Two-tailed one sample t-test; Acute GST n = 6; Acute MST n = 6; Chronic GST n = 5, Chronic MST n = 10. **d**, Protein expression of PDHK1 as determined by western blot analysis. Ordinary one-way ANOVA; n = 7. **e**, Protein expression of phosphorylated PDHE1 α (ser239) as determined by western blot analysis. Ordinary one-way ANOVA; n = 7. **f**, Protein expression of PDHc as determined by western blot analysis. Ordinary one-way ANOVA; n = 8. **g**, Glucose uptake by human CD8⁺ T cells treated with DEG. Data represented as relative light units (RLU). Mixed-effects analysis; n = 9 (acute), n = 14 (chronic). **h**, **q** PCR analysis of CD8⁺ T cells treated with DEG for 7 days. Each dot represents one human donor relative to untreated donor control (dotted black line), normalised to HPRT. Two-tailed one sample t-test; FASN

n = 4, FASBP n = 4; CPT1A n = 3. **i**, Model of mitochondrial fuel flexibility tests and illustration of calculations used to determine mitochondrial fuel oxidative capacity and dependency. (*Adapted from BioRender.com*) **j**, Fatty acid oxidation dependency as determined by OCR measurements during a mitochondrial fuel flex test of CD8⁺ T cells treated with +/- DEG 500 μ M for 7 days as described in Extended Data Fig. 4i. Calculated percentage fatty acid dependency (right): Two-tailed paired t-test; n = 5. **k**, OCR measurements and percentage fuel oxidative capacity (cap) or dependency (dep) during a mitochondrial fuel flex test of CD8⁺ T cells treated with +/- DEG 500 μ M for 7 days, as described in Extended Data Fig. 4i. Calculated percentage fuel capacity and dependency (bottom): Two-tailed paired t-test; Glucose oxidation dependency n = 6; Glucose oxidation capacity n = 5; Glutamine oxidation dependency n = 5; Glutamine oxidation capacity n = 6. All experiment describes used 500 μ M DEG. All scatter plots show median and 95% CI where each dot represents one human donor. OCR time course graphs show Mean and Error with 95% CI.



Extended Data Fig. 5 | See next page for caption.

Extended Data Fig. 5 | Glutarate reduces tumor growth and increases T cell numbers and tumor infiltration. **a**, Cell count of human CAR-T cells treated +/- 500 μ M for 7 days. Two-tailed paired t-test; n = 6. **b**, Cell count of murine OT1 CD8⁺ T cells treated +/- 500 μ M for 7 days. Two-tailed paired t-test; n = 6. **c**, *In vitro* B16F10-OVA cell growth +/- DEG 500 μ M as determined by cell counting and represented as log₂ FC. One way ANOVA; n = 3. **d**, Cell count of different cancer cell lines treated with increasing concentrations of DEG for 72 h. Cell count relative to appropriate untreated control. One way ANOVA; n = 3. **e**, Cell count of human HER2-CAR-T_shRNA cell numbers 7 days post transduction. Two-tailed paired t-test; n = 4. **f**, Gating strategy used for analysis of Fig. 5-m and Extended Data Fig. 5g. **g**, Frequency of immune cell types in

peripheral blood, tumor, spleen, and tumor draining lymph nodes, 14 days post tumor inoculation, represented as log₂ FC relative to CD45⁺ count. Two-tailed unpaired t-test; Tumor CT n = 10; Tumor DEG n = 8; Peripheral Blood CT + DEG n = 15; Spleen CT + DEG n = 15; Tumor Draining Lymph Nodes CT n = 15; Tumor Draining Lymph Nodes DEG n = 15. **h**, Percentage of CD8⁺/CD4⁺ T cells expressing CD44/CD62L in tumors 14 days post tumor inoculation. Two-tailed unpaired t-test; Ct n = 20; DEG n = 18. **i**, MFI of TIM3, PD1, LAG3 and TOX on CD8⁺/CD4⁺ T cells in tumors, 14 days post tumor inoculation. Two-tailed unpaired t-test; n = 10. Graph shows median + 95% CI where each dot represents one murine or human donor as indicated. *p < 0.05, **p < 0.01.

Reporting Summary

Nature Portfolio wishes to improve the reproducibility of the work that we publish. This form provides structure for consistency and transparency in reporting. For further information on Nature Portfolio policies, see our [Editorial Policies](#) and the [Editorial Policy Checklist](#).

Statistics

For all statistical analyses, confirm that the following items are present in the figure legend, table legend, main text, or Methods section.

- | n/a | Confirmed |
|-------------------------------------|--|
| <input type="checkbox"/> | <input checked="" type="checkbox"/> The exact sample size (n) for each experimental group/condition, given as a discrete number and unit of measurement |
| <input type="checkbox"/> | <input checked="" type="checkbox"/> A statement on whether measurements were taken from distinct samples or whether the same sample was measured repeatedly |
| <input type="checkbox"/> | <input checked="" type="checkbox"/> The statistical test(s) used AND whether they are one- or two-sided
<i>Only common tests should be described solely by name; describe more complex techniques in the Methods section.</i> |
| <input type="checkbox"/> | <input checked="" type="checkbox"/> A description of all covariates tested |
| <input type="checkbox"/> | <input checked="" type="checkbox"/> A description of any assumptions or corrections, such as tests of normality and adjustment for multiple comparisons |
| <input type="checkbox"/> | <input checked="" type="checkbox"/> A full description of the statistical parameters including central tendency (e.g. means) or other basic estimates (e.g. regression coefficient) AND variation (e.g. standard deviation) or associated estimates of uncertainty (e.g. confidence intervals) |
| <input type="checkbox"/> | <input checked="" type="checkbox"/> For null hypothesis testing, the test statistic (e.g. F , t , r) with confidence intervals, effect sizes, degrees of freedom and P value noted
<i>Give P values as exact values whenever suitable.</i> |
| <input checked="" type="checkbox"/> | <input type="checkbox"/> For Bayesian analysis, information on the choice of priors and Markov chain Monte Carlo settings |
| <input checked="" type="checkbox"/> | <input type="checkbox"/> For hierarchical and complex designs, identification of the appropriate level for tests and full reporting of outcomes |
| <input checked="" type="checkbox"/> | <input type="checkbox"/> Estimates of effect sizes (e.g. Cohen's d , Pearson's r), indicating how they were calculated |

Our web collection on [statistics for biologists](#) contains articles on many of the points above.

Software and code

Policy information about [availability of computer code](#)

- | | |
|-----------------|--|
| Data collection | Aurora (Cytek Biosciences); Aria III (BD Biosciences); microplate reader (Sunrise, Tecan Austria GmbH); Waters Acquity UPLC system coupled to a Xevo-TQ-S mass spectrometer (Waters, Milford, MA, USA); StepOnePlus system (Applied Biosystems); iBrightCL1000 (Thermo Fisher); Q Exactive HF hybrid Orbitrap mass spectrometer (Thermo Fisher Scientific); an Orbitrap Fusion Lumos coupled to an Ultimate 3000 RSLC nano UHPLC equipped with a 100 μ m ID x 2 cm Acclaim PepMap Precolumn (Thermo Fisher Scientific); Seahorse XFe bioanalyser (Agilent); on FLUROstar Omega (BMG Labtech) |
| Data analysis | FlowJo_V10.7.2; Mascot Server v.2.5.1 (Matrix Science Ltd., UK); PEAKS Studio (version 8.0, Bioinformatics Solutions Inc.); Prism 9 software (GraphPad); iBright Analysis Software_V4.0.1; ImageJ; |

For manuscripts utilizing custom algorithms or software that are central to the research but not yet described in published literature, software must be made available to editors and reviewers. We strongly encourage code deposition in a community repository (e.g. GitHub). See the Nature Portfolio [guidelines for submitting code & software](#) for further information.

Data

Policy information about [availability of data](#)

All manuscripts must include a [data availability statement](#). This statement should provide the following information, where applicable:

- Accession codes, unique identifiers, or web links for publicly available datasets
- A description of any restrictions on data availability
- For clinical datasets or third party data, please ensure that the statement adheres to our [policy](#)

All data generated or analysed during this study are included in the published article and its supplementary information files. The data that support the findings of this study are available from the corresponding author upon reasonable request. Source data are provided with this paper

Human research participants

Policy information about [studies involving human research participants and Sex and Gender in Research](#).

Reporting on sex and gender	Sex and gender of healthy volunteer blood donors was not obtained as per ethical approval requirements.
Population characteristics	Human peripheral blood mononuclear cells (PBMCs) were obtained from National Health Service (NHS) Blood and Transplant (NHSBT: Addenbrooke's Hospital, Cambridge, United Kingdom) or Karolinska Hospital Service, Sweden. All volunteers were healthy as defined by national blood donation standards and over the age of 18.
Recruitment	Human peripheral blood mononuclear cells (PBMCs) were obtained from National Health Service (NHS) Blood and Transplant (NHSBT: Addenbrooke's Hospital, Cambridge, United Kingdom) or Karolinska Hospital Service, Sweden, from healthy volunteers between the ages of 20 and 40.
Ethics oversight	Ethical approval was obtained from the East of England-Cambridge Central Research Ethics Committee (06/Q0108/281) .

Note that full information on the approval of the study protocol must also be provided in the manuscript.

Field-specific reporting

Please select the one below that is the best fit for your research. If you are not sure, read the appropriate sections before making your selection.

- Life sciences Behavioural & social sciences Ecological, evolutionary & environmental sciences

For a reference copy of the document with all sections, see [nature.com/documents/nr-reporting-summary-flat.pdf](https://www.nature.com/documents/nr-reporting-summary-flat.pdf)

Life sciences study design

All studies must disclose on these points even when the disclosure is negative.

Sample size	Power calculations were carried out where effect size could be estimated.
Data exclusions	Mice who did not grow tumors were excluded from the study. For in-vitro studies, data point identified as an outlier by independent analysis using Prism Software were excluded.
Replication	All experiments were replicated in at least three independent studies with the following exceptions: 1. Extended Data Fig. 1m: This was repeated independently 3 times but an error was made with one sample during the final derivation for mass spectrometry. Thus, only two independent results are reported. 2. Fig 5f: This experiment was performed independently twice with the same result observed both times. It was not performed a third time due to the significant cost involved and the desire to keep use of animals to a minimum. 3. Fig. 5m and Extended Data Fig. 5g-i: This experiment was performed independently once with at least 8 biological replicates per group (i.e. animals). Tumor growth and blood sampling was performed in at least 3 independent studies however, terminal experiments (tumor, spleen and lymph node analysis) was only performed once. In Fig. 1m all animals displayed the same trend. Power calculations were carried out to estimate effect size.
Randomization	Randomization for in vitro studies was not possible as groups were separated based on treatment. Randomization was preformed for in vivo studies. In animal studies, mice were randomly assigned groups using an Online random number generator.
Blinding	In vitro studies were not blinded as they all required specific culture conditions for treatment groups. Blinding in the animal experiments was not possible as animals were separated based on treatment type. Analysis of blood and tissues from animal experiments was blinded.

Behavioural & social sciences study design

All studies must disclose on these points even when the disclosure is negative.

Study description	Briefly describe the study type including whether data are quantitative, qualitative, or mixed-methods (e.g. qualitative cross-sectional, quantitative experimental, mixed-methods case study).
Research sample	State the research sample (e.g. Harvard university undergraduates, villagers in rural India) and provide relevant demographic information (e.g. age, sex) and indicate whether the sample is representative. Provide a rationale for the study sample chosen. For studies involving existing datasets, please describe the dataset and source.
Sampling strategy	Describe the sampling procedure (e.g. random, snowball, stratified, convenience). Describe the statistical methods that were used to predetermine sample size OR if no sample-size calculation was performed, describe how sample sizes were chosen and provide a rationale for why these sample sizes are sufficient. For qualitative data, please indicate whether data saturation was considered, and what criteria were used to decide that no further sampling was needed.
Data collection	Provide details about the data collection procedure, including the instruments or devices used to record the data (e.g. pen and paper, computer, eye tracker, video or audio equipment) whether anyone was present besides the participant(s) and the researcher, and whether the researcher was blind to experimental condition and/or the study hypothesis during data collection.
Timing	Indicate the start and stop dates of data collection. If there is a gap between collection periods, state the dates for each sample cohort.
Data exclusions	If no data were excluded from the analyses, state so OR if data were excluded, provide the exact number of exclusions and the rationale behind them, indicating whether exclusion criteria were pre-established.
Non-participation	State how many participants dropped out/declined participation and the reason(s) given OR provide response rate OR state that no participants dropped out/declined participation.
Randomization	If participants were not allocated into experimental groups, state so OR describe how participants were allocated to groups, and if allocation was not random, describe how covariates were controlled.

Ecological, evolutionary & environmental sciences study design

All studies must disclose on these points even when the disclosure is negative.

Study description	Briefly describe the study. For quantitative data include treatment factors and interactions, design structure (e.g. factorial, nested, hierarchical), nature and number of experimental units and replicates.
Research sample	Describe the research sample (e.g. a group of tagged <i>Passer domesticus</i> , all <i>Stenocereus thurberi</i> within Organ Pipe Cactus National Monument), and provide a rationale for the sample choice. When relevant, describe the organism taxa, source, sex, age range and any manipulations. State what population the sample is meant to represent when applicable. For studies involving existing datasets, describe the data and its source.
Sampling strategy	Note the sampling procedure. Describe the statistical methods that were used to predetermine sample size OR if no sample-size calculation was performed, describe how sample sizes were chosen and provide a rationale for why these sample sizes are sufficient.
Data collection	Describe the data collection procedure, including who recorded the data and how.
Timing and spatial scale	Indicate the start and stop dates of data collection, noting the frequency and periodicity of sampling and providing a rationale for these choices. If there is a gap between collection periods, state the dates for each sample cohort. Specify the spatial scale from which the data are taken
Data exclusions	If no data were excluded from the analyses, state so OR if data were excluded, describe the exclusions and the rationale behind them, indicating whether exclusion criteria were pre-established.
Reproducibility	Describe the measures taken to verify the reproducibility of experimental findings. For each experiment, note whether any attempts to repeat the experiment failed OR state that all attempts to repeat the experiment were successful.
Randomization	Describe how samples/organisms/participants were allocated into groups. If allocation was not random, describe how covariates were controlled. If this is not relevant to your study, explain why.
Blinding	Describe the extent of blinding used during data acquisition and analysis. If blinding was not possible, describe why OR explain why blinding was not relevant to your study.

Did the study involve field work? Yes No

Reporting for specific materials, systems and methods

We require information from authors about some types of materials, experimental systems and methods used in many studies. Here, indicate whether each material, system or method listed is relevant to your study. If you are not sure if a list item applies to your research, read the appropriate section before selecting a response.

Materials & experimental systems

n/a	Involvement	Material/System
<input type="checkbox"/>	<input checked="" type="checkbox"/>	Antibodies
<input type="checkbox"/>	<input checked="" type="checkbox"/>	Eukaryotic cell lines
<input checked="" type="checkbox"/>	<input type="checkbox"/>	Palaeontology and archaeology
<input type="checkbox"/>	<input checked="" type="checkbox"/>	Animals and other organisms
<input checked="" type="checkbox"/>	<input type="checkbox"/>	Clinical data
<input checked="" type="checkbox"/>	<input type="checkbox"/>	Dual use research of concern

Methods

n/a	Involvement	Method
<input checked="" type="checkbox"/>	<input type="checkbox"/>	ChIP-seq
<input type="checkbox"/>	<input checked="" type="checkbox"/>	Flow cytometry
<input checked="" type="checkbox"/>	<input type="checkbox"/>	MRI-based neuroimaging

Antibodies

Antibodies used

Antibody	Company	Catalogue Number	Dilution		
anti-5hmC Active Motif		10013602			
anti-PDHK1 cell signalling		3820	1:1000		
anti-PPIB cell signalling		43603	1:1000		
anti-Phospho-PDH a1 cell signalling		37115	1:1000		
anti-SIRT5 cell signalling		87795	1:1000		
anti-H3 cell signalling		4499	1:1000		
anti-H3K4me2 cell signalling		9725	1:1000		
anti-H3K4me3 cell signalling		9751	1:1000		
anti-H3K9me2 cell signalling		4658	1:1000		
anti-H3K9me3 cell signalling		13969	1:1000		
anti-H3K27me2 cell signalling		9728	1:1000		
anti-H3K27me3 cell signalling		9733	1:1000		
anti-H3K36me2 cell signalling		2901	1:1000		
anti-H3K36me3 cell signalling		4909	1:1000		
anti-H3K79me2 cell signalling		5427	1:1000		
anti-H3K79me3 cell signalling		4360	1:1000		
anti-b-actin cell signalling		122625	1:1000		
PDHc	Thermo Scientific	456799	1:1000		
GCDH	Thermo Scientific	PA5-60294	1:1000		
anti-lipoic acid	Sigma	437695	1:1000		
pan anti-glutaryllysine	PTM Biolabs	PTM-1151	1:1000		
Anti-OGDH cell signalling		26865S	1:1000		
Anti-DLAT cell signalling		12362S	1:1000		
Rabbit IgG HPR R&D	HAF008		1:5000		
Mouse IgG HPR R&D	HAF009		1:1000		
Antibody	Fluorophore	Clone	Company	Catalogue Number	Dilution
CCR7 PE	3D12	BD	Biosciences	552176	1:100
CCR7 PE/Cy7	3D12	BD	Biosciences	557648	1:100
CD127 PE	A019D5	Biolegend		351303	1:200
CD127 APC	A019D5	Biolegend		351342	1:200
CD137 PE	4B4-1	Biolegend		309804	1:200
CD19 PE	4G7	Biolegend		392505	1:200
CD19 APC	4G7	Biolegend		392504	1:200
CD25 BV510	BC96	Biolegend		302639	1:200
CD27 PerCP/Cy5.5	M-T271	Biolegend		356408	1:200
CD3 BV510	HIT3a	BD	Biosciences	564713	1:200
CD34 (RQR8)	AF488	QEnd10	R&D	FAB7227G	1:100
CD44 FITC	BJ18	Biolegend		338803	1:200
CD45RA BV650	HI101	Biolegend		304135	1:200
CD45RO	BUV496	UCHL1	BD	Biosciences	749888
					1:200
CD45RO	BV605	UCHL1	Biolegend	304238	1:200
CD62L	AF488	DREG-56	Biolegend	304816	1:200
CD62L	PerCP/Cy5.5	DREG-56	Biolegend	304824	1:200
CD8a	BUV395	RPA-T8	BD	563796	

1:400
 CD8a AF700 HIT8a Biolegend 300920 1:400
 CD95 PerCP/Cy5.5 DX2 Biolegend 305630 1:200
 GzmB PerCP/Cy5.5 QA16A02 Biolegend 372211 1:200
 GzmB AF647 GB11 Biolegend 515405 1:200
 LAG3 (CD223) AF647 11C3C65 Biolegend 369304 1:200
 Perforin Pacific Blue dG9 Biolegend 308117
 1:200
 Perforin PerCP/Cy5.5 dG9 Biolegend 308114 1:200
 TBET PerCP/Cy5.5 4B10 Biolegend 644805 1:200
 TBET PE/Dazzle594 4B10 Biolegend 644828
 1:200
 TCF1 PE S33-966 BD Biosciences 564217
 1:200
 TIGIT (VSTM3) PE/Cy7 A15153G Biolegend 372713 1:200
 TIM3 (CD366) BV605 F38-2E2 Biolegend 345017 1:200
 TOX eFluor660 TXRX10 eBiosciences 50-6502-82 1:200
 Antibody Fluorophore Clone Company Catalogue Number Dilution
 CD11b AF647 M1/70 Biolegend 101220 1:200
 CD11b AF488 M1/70 eBiosciences 53-0112-80 1:200
 CD11b AF700 M1/70 eBiosciences 56-0112-80 1:200
 CD11c PerCP/Cy5.5 N418 eBiosciences 45-0114-80 1:200
 CD127 AF647 A7R34 Biolegend 135020 1:200
 CD137 PE 17B5 Biolegend 106105 1:200
 CD137 APC 17B5 Biolegend 106110 1:200
 CD19 FITC eBio1D3 eBiosciences 11-0193-82 1:200
 CD19 PE eBio1D3 eBiosciences 25-0193-82 1:200
 CD19 APC eBio1D3 eBiosciences 17-0193-82 1:200
 CD25 PE PC61.5 eBiosciences 12-0261-818 1:200
 CD27 AF700 LG.3A10 Biolegend 124239 1:200
 CD34 AF647 HM34 Biolegend 128605 1:200
 CD3 PE/Dazzle 17A2 Biolegend 100245 1:200
 CD4 BV421 GK1.5 Biolegend 100437 1:200
 CD4 AF488 GK1.5 Biolegend 100423 1:200
 CD4 BV650 RM4-5 Biolegend 100545 1:200
 CD4 BV510 GK1.5 Biolegend 100449 1:200
 CD44 PerCP/Cy5.5 IM7 Biolegend 103032 1:200
 CD44 BUV496 IM7 BD Biosciences 741057 1:200
 CD45.1 PerCP/Cy5.5 A20 eBiosciences 45-0453-82 1:200
 CD45.1 PE A20 Biolegend 110708 1:200
 CD45.2 AF488 104 Biolegend 109815 1:200
 CD45.2 BV421 104 BD Biosciences 562895 1:200
 CD62L AF488 MEL-14 Biolegend 104419 1:200
 CD62L PE MEL-14 Biolegend 104408 1:200
 CD62L AF488 DREG-56 Biolegend 304816 1:200
 CD62L BUV737 MEL-14 BD Biosciences 612833 1:200
 CD8a BUV395 53-6.7 BD Biosciences 565968 1:400
 CD8a AF700 53-6.7 Biolegend 100730 1:400
 CD8a BV510 53-6.7 Biolegend 100751 1:400
 CTLA4(CD152) PerCP/Cy5.5 UC10-4B9 Biolegend 106315 1:200
 GzmB PerCP/Cy5.5 AD2 Biolegend 344013 1:200
 LAG3(CD223) PerCP/Cy5.5 C9B7W Biolegend 125212 1:200
 LAG3(CD223) PE C9B7W BD Biosciences 552380 1:200
 PD-1(CD279) PerCP-eFluorTM 710 J43 Thermo Scientific 46-9985-82 1:200
 Perforin APC eBioOMAK-D Biolegend 17-9392-80 1:200
 TBET PerCP/Cy5.5 4B10 Biolegend 644805 1:200
 TCF1 PE S33-966 BD 564217
 1:200
 TIM3(CD366) BV605 RMT3-23 Biolegend 119721 1:200
 TIM3(CD366) BV605 F38-2E2 Biolegend 345017 1:200
 TOX APC TXRX10 eBiosciences 50-6502-82 1:200
 TCRgd BV421 RUO Biolegend 118119 1:200
 Ly6G BV605 1A8 Biolegend 127639 1:200
 Ly6C PE/Cy7 HK1.4 Biolegend 128017 1:200
 MHC II BV650 M5/14.15.2 Biolegend 107641 1:200
 NK1.1 PE PK136 Biolegend 108726 1:200

Validation

All antibodies were purchased from commercial companies as indicated. Antibodies were validated by cited companies. No unvalidated antibody was used in this study.

Eukaryotic cell lines

Policy information about [cell lines and Sex and Gender in Research](#)

Cell line source(s)	B16-F10 ATCC (CEL-6475); HEK293T from Takara (632180) ; SKOV3 from ATCC (HTB-77); Raji-GFP-Luc cells from Biocytogen (B-HCL-010) ; Jurkat from ATCC (TIB-152) ; RAW 264.7 rom ATCC (TIB-71); HeLa gift from Prof. Paul Lehner (University of Cambridge);
Authentication	B16-F10, SKOV3 and Raji cells were authenticated using cell surface antigen expression RAW, and HEK293 cells were not authenticated further than ensuring they looked and grew according to published data. HeLa cells were authenticated by short tandem repeat profiling (Eurofins Genomics).
Mycoplasma contamination	Cells tested negative for mycoplasma contamination.
Commonly misidentified lines (See ICLAC register)	<p>The following cell lines used in this study are reported by the International Cell Line Authentication Committee (https://iclac.org/databases/cross-contaminations/) as known misidentified cell lines:</p> <ol style="list-style-type: none"> 1. HEK293T 2. Raji 3. Jurkat 4. Raw 264.7 5. HeLa <p>Each of these cell lines (except for HeLa and Raw 264.7 cells) were commercially purchased for the purpose of this study. Authenticity of each cell line was confirmed by the supplier prior to purchase. Supplier information is provided in the methods section.</p> <p>HeLa cells were authenticated by short tandem repeat profiling (Eurofins Genomics).</p>

Palaeontology and Archaeology

Specimen provenance	<i>Provide provenance information for specimens and describe permits that were obtained for the work (including the name of the issuing authority, the date of issue, and any identifying information). Permits should encompass collection and, where applicable, export.</i>
Specimen deposition	<i>Indicate where the specimens have been deposited to permit free access by other researchers.</i>
Dating methods	<i>If new dates are provided, describe how they were obtained (e.g. collection, storage, sample pretreatment and measurement), where they were obtained (i.e. lab name), the calibration program and the protocol for quality assurance OR state that no new dates are provided.</i>
<input type="checkbox"/> Tick this box to confirm that the raw and calibrated dates are available in the paper or in Supplementary Information.	
Ethics oversight	<i>Identify the organization(s) that approved or provided guidance on the study protocol, OR state that no ethical approval or guidance was required and explain why not.</i>

Note that full information on the approval of the study protocol must also be provided in the manuscript.

Animals and other research organisms

Policy information about [studies involving animals; ARRIVE guidelines](#) recommended for reporting animal research, and [Sex and Gender in Research](#)

Laboratory animals	<p>C57BL/6J animals (632, Charles River), were used in in vitro assays and in orthotopic tumor growth and infiltration experiments (male and female mice used; 8-12 weeks of age). NOD.Cg-Prkdcscidll2rgtm1Wjl/SzJ mice (005557, The Jackson Laboratory) were used in human CAR-T cell experiments. Donor TCR-transgenic OT1 mice (003831, The Jackson Laboratory) were crossed with mice bearing the CD45.1 congenic marker (002014, The Jackson Laboratory). Targeted deletion of HIF1 in T cells was achieved by crossing homozygous mice carrying loxP-flanked alleles Hif1 61 into a mouse strain of cre recombinase expression driven by the distal promoter of the lymphocyte-specific Lck gene (012837, The Jackson Laboratory). All the experiments were performed with age and sex matched cre negative controls. TCR-transgenic OT1 mice and mice with targeted deletion of HIF1 in T cells were bred and housed in specific pathogen-free conditions in accordance with the regional animal ethics Committee of Northern Stockholm, Sweden. All animal experiments were performed in accordance with the ethical regulation of the UK Home Office and the University of Cambridge and/or the regional animal ethics Committee of Northern Stockholm, Sweden.</p> <p>Housing conditions were as follows: 12 hour light cycle with gradual change. Temperature; 22-23°C. Humidity; 50%.</p>
Wild animals	No wild animals were used in this study.
Reporting on sex	Female and male mice were used in in vitro and in vivo studies. No sex or gender differences were observed.

Field-collected samples

Ethics oversight

Note that full information on the approval of the study protocol must also be provided in the manuscript.

Clinical data

Policy information about [clinical studies](#)

All manuscripts should comply with the ICMJE [guidelines for publication of clinical research](#) and a completed [CONSORT checklist](#) must be included with all submissions.

Clinical trial registration

Study protocol

Data collection

Outcomes

Dual use research of concern

Policy information about [dual use research of concern](#)

Hazards

Could the accidental, deliberate or reckless misuse of agents or technologies generated in the work, or the application of information presented in the manuscript, pose a threat to:

- | No | Yes | |
|-------------------------------------|--------------------------|----------------------------|
| <input checked="" type="checkbox"/> | <input type="checkbox"/> | Public health |
| <input checked="" type="checkbox"/> | <input type="checkbox"/> | National security |
| <input checked="" type="checkbox"/> | <input type="checkbox"/> | Crops and/or livestock |
| <input checked="" type="checkbox"/> | <input type="checkbox"/> | Ecosystems |
| <input checked="" type="checkbox"/> | <input type="checkbox"/> | Any other significant area |

Experiments of concern

Does the work involve any of these experiments of concern:

- | No | Yes | |
|-------------------------------------|--------------------------|---|
| <input checked="" type="checkbox"/> | <input type="checkbox"/> | Demonstrate how to render a vaccine ineffective |
| <input checked="" type="checkbox"/> | <input type="checkbox"/> | Confer resistance to therapeutically useful antibiotics or antiviral agents |
| <input checked="" type="checkbox"/> | <input type="checkbox"/> | Enhance the virulence of a pathogen or render a nonpathogen virulent |
| <input checked="" type="checkbox"/> | <input type="checkbox"/> | Increase transmissibility of a pathogen |
| <input checked="" type="checkbox"/> | <input type="checkbox"/> | Alter the host range of a pathogen |
| <input checked="" type="checkbox"/> | <input type="checkbox"/> | Enable evasion of diagnostic/detection modalities |
| <input checked="" type="checkbox"/> | <input type="checkbox"/> | Enable the weaponization of a biological agent or toxin |
| <input checked="" type="checkbox"/> | <input type="checkbox"/> | Any other potentially harmful combination of experiments and agents |

ChIP-seq

Data deposition

- Confirm that both raw and final processed data have been deposited in a public database such as [GEO](#).
- Confirm that you have deposited or provided access to graph files (e.g. BED files) for the called peaks.

Data access links
May remain private before publication.

Files in database submission

Genome browser session (e.g. [UCSC](#))

Methodology

Replicates	<i>Describe the experimental replicates, specifying number, type and replicate agreement.</i>
Sequencing depth	<i>Describe the sequencing depth for each experiment, providing the total number of reads, uniquely mapped reads, length of reads and whether they were paired- or single-end.</i>
Antibodies	<i>Describe the antibodies used for the ChIP-seq experiments; as applicable, provide supplier name, catalog number, clone name, and lot number.</i>
Peak calling parameters	<i>Specify the command line program and parameters used for read mapping and peak calling, including the ChIP, control and index files used.</i>
Data quality	<i>Describe the methods used to ensure data quality in full detail, including how many peaks are at FDR 5% and above 5-fold enrichment.</i>
Software	<i>Describe the software used to collect and analyze the ChIP-seq data. For custom code that has been deposited into a community repository, provide accession details.</i>

Flow Cytometry

Plots

Confirm that:

- The axis labels state the marker and fluorochrome used (e.g. CD4-FITC).
- The axis scales are clearly visible. Include numbers along axes only for bottom left plot of group (a 'group' is an analysis of identical markers).
- All plots are contour plots with outliers or pseudocolor plots.
- A numerical value for number of cells or percentage (with statistics) is provided.

Methodology

Sample preparation

Single cell suspensions were stained with Near-IR Dead Cell Stain Kit (10119, Thermo Fisher) followed by surface and intracellular staining with fluorochrome-labelled antibodies (Supplementary Table 1). Staining of cytoplasmic and nuclear antigens was performed using the Fixation/Permeabilization kit (554714, BD Biosciences) and the Transcription Factor buffer set (562725, BD Biosciences), respectively. For proliferation assays, cells were loaded with Cell Trace Violet (C34557, Thermo Fisher) according to manufacturer's instructions. Samples were acquired on an Aurora (Cytek Biosciences). For 5hmC staining, cells were stained for surface antigens as above and then fixed and permeabilised with the Transcription Factor buffer set (562725, BD Biosciences). Next cells were incubated with 4M HCL for 10 min at room temperature. The cells were then thoroughly washed and incubated in blocking buffer (0.1% PBS-Triton, 5% FBS) for 30min at 4oC. The cells were then incubated with primary anti-5hmC (10013602; Active Motif) overnight at 4oC and the day after with secondary antibody for 1 hr at room temperature. Flow cytometry was then performed as explained above.

Single cell suspensions were stained with Near-IR Dead Cell Stain Kit (10119, Thermo Fisher) followed by surface and intracellular staining with fluorochrome-labelled antibodies (Supplementary Table 1). Staining of cytoplasmic and nuclear antigens was performed using the Fixation/Permeabilization kit (554714, BD Biosciences) and the Transcription Factor buffer set (562725, BD Biosciences), respectively. For proliferation assays, cells were loaded with Cell Trace Violet (C34557, Thermo Fisher) according to manufacturer's instructions. Samples were acquired on an Aurora (Cytek Biosciences). For 5hmC staining, cells were stained for surface antigens as above and then fixed and permeabilised with the Transcription Factor buffer set (562725, BD Biosciences). Next cells were incubated with 4M HCL for 10 min at room temperature. The cells were then thoroughly washed and incubated in blocking buffer (0.1% PBS-Triton, 5% FBS) for 30min at 4oC. The cells were then incubated with primary anti-5hmC (10013602; Active Motif) overnight at 4oC and the day after with secondary antibody for 1 hr at room temperature. Flow cytometry was then performed as explained above.

Single cell suspensions were stained with Near-IR Dead Cell Stain Kit (10119, Thermo Fisher) followed by surface and intracellular staining with fluorochrome-labelled antibodies (Supplementary Table 1). Staining of cytoplasmic and nuclear antigens was performed using the Fixation/Permeabilization kit (554714, BD Biosciences) and the Transcription Factor buffer set (562725, BD Biosciences), respectively. For proliferation assays, cells were loaded with Cell Trace Violet (C34557, Thermo Fisher) according to manufacturer's instructions. Samples were acquired on an Aurora (Cytek Biosciences). For 5hmC staining, cells were stained for surface antigens as above and then fixed and permeabilised with the Transcription Factor buffer set (562725, BD Biosciences). Next cells were incubated with 4M HCL for 10 min at room temperature. The cells were then thoroughly washed and incubated in blocking buffer (0.1% PBS-Triton, 5% FBS) for 30min at 4oC. The cells were then incubated with primary anti-5hmC (10013602; Active Motif) overnight at 4oC and the day after with secondary antibody for 1 hr at room temperature. Flow cytometry was then performed as explained above.

Single cell suspensions were stained with Near-IR Dead Cell Stain Kit (10119, Thermo Fisher) followed by surface and intracellular staining with fluorochrome-labelled antibodies (Supplementary Table 1). Staining of cytoplasmic and nuclear antigens was performed using the Fixation/Permeabilization kit (554714, BD Biosciences) and the Transcription Factor buffer set (562725, BD Biosciences), respectively. For proliferation assays, cells were loaded with Cell Trace Violet (C34557, Thermo Fisher) according to manufacturer's instructions. Samples were acquired on an Aurora (Cytek Biosciences).

Instrument	Aurora (Cytek Biosciences).
Software	FlowJo

Cell population abundance

Gating strategy

Tick this box to confirm that a figure exemplifying the gating strategy is provided in the Supplementary Information.

Magnetic resonance imaging

Experimental design

Design type

Design specifications

Behavioral performance measures

Acquisition

Imaging type(s)

Field strength

Sequence & imaging parameters

Area of acquisition

Diffusion MRI Used Not used

Preprocessing

Preprocessing software

Normalization

Normalization template

Noise and artifact removal

Volume censoring

Statistical modeling & inference

Model type and settings

Effect(s) tested

Specify type of analysis: Whole brain ROI-based Both

Statistic type for inference (See [Eklund et al. 2016](#))

Correction

Models & analysis

n/a | Involved in the study

Functional and/or effective connectivity

Graph analysis

Multivariate modeling or predictive analysis

Functional and/or effective connectivity

Report the measures of dependence used and the model details (e.g. Pearson correlation, partial correlation, mutual information).

Graph analysis

Report the dependent variable and connectivity measure, specifying weighted graph or binarized graph, subject- or group-level, and the global and/or node summaries used (e.g. clustering coefficient, efficiency, etc.).

Multivariate modeling and predictive analysis

Specify independent variables, features extraction and dimension reduction, model, training and evaluation metrics.